CHALMERS
UNIVERSITY OF TECHNOLOGY

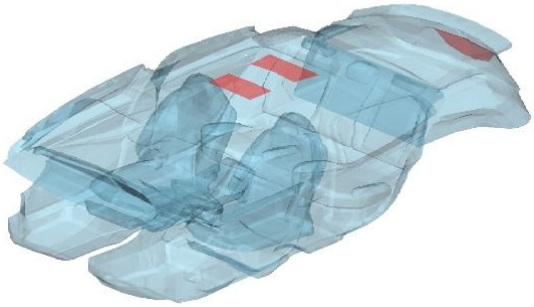

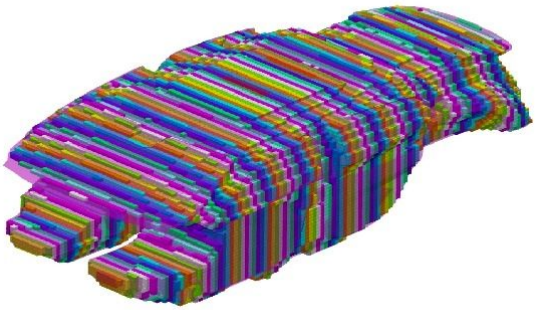

Development and optimization of climate- and energy related models in electromobility using thermal comfort and CFD

A modeling approach using coupling of 1D- and 3D-CFD

Master's thesis in Sustainable Energy Systems - MPSES

OLA LÖSETH

DEPARTMENT OF MECHANICS AND MARITIME SCIENCES

CHALMERS UNIVERSITY OF TECHNOLOGY
Gothenburg, Sweden 2022
www.chalmers.se

Master's thesis 2022:22

Development and optimization of climate- and energy related models in electromobility using thermal comfort and CFD

OLA LÖSETH

CHALMERS
UNIVERSITY OF TECHNOLOGY

Department of Mechanics and Maritime Sciences
Division of Vehicle Engineering and Autonomous Systems
Chalmers University of Technology
Gothenburg, Sweden 2022

Development and optimization of climate- and energy related models in electromobility using thermal comfort and CFD
OLA LÖSETH

Supervisor: Martin Forsell, CEVT
Supervisor: Simone Sebben, Department of Mechanics and Maritime Sciences
Examiner: Simone Sebben, Department of Mechanics and Maritime Sciences

Master's Thesis 2022:22
Department of Mechanics and Maritime Sciences
Division of Vehicle Engineering and Autonomous Systems
Chalmers University of Technology
SE-412 96 Gothenburg
Telephone +46 31 772 1000

Cover: Cabin volume discretization performed in GEM3D.

Typeset in LaTeX
Printed by Chalmers Reproservice
Gothenburg, Sweden 2022

Development and optimization of climate- and energy related models in electromobility using thermal comfort and CFD
OLA LÖSETH
Department of Mechanics and Maritime Sciences
Chalmers University of Technology

Abstract

Increasing environmental pressure on the automotive industry has resulted in growing efforts to develop sustainable alternatives, among them electric vehicles. Climatization of electric vehicles has been shown to be energy intensive as electric motors do not produce much waste heat. As a result, optimizing the cabin climatization is of great importance, and the purpose of this thesis project is to provide a method capable of evaluating the climate of a vehicle cabin. This project is in collaboration with CEVT, an innovation center that is strongly connected to the vehicle industry. The objective of the thesis is to develop a method that, with the utilization of computational fluid dynamics and thermal comfort modeling, can evaluate the cabin climate to enable energy optimization of the thermal system. The method is developed by utilizing and combining CFD and thermal solvers with the Berkeley Comfort Model to build a virtual cabin environment that can predict the thermal comfort of cabin occupants. The cabin model is also integrated into a system simulation environment representative of the complete vehicle thermal system. The project resulted in a simulation environment capable of assessing the thermal comfort of passengers occupying the vehicle cabin. Furthermore, the study has indicated that the climatization process can be adjusted based on the clothing of the passengers to obtain a significant decrease in energy use.

Keywords: climatization, electric vehicle, CEVT, cabin climate, modeling, CFD, heat transfer, Berkeley Comfort Model, thermal comfort.

Acknowledgements

First, I would like to express that I am incredibly grateful to my supervisor Martin Forsell, who supported me with my thesis work from the very beginning. Furthermore, I would like to thank the rest of the system simulations team at CEVT, who has included me in the team and supported me greatly throughout this thesis, and for that I am extremely grateful. I am especially grateful to Léon Löwered, who recruited me and made this thesis possible. I would also like to thank Chanin Lerdmaleewong, who shared his technical expertise within system simulations during the difficult times of this thesis project.

Lastly, I would like to thank my examiner Simone Sebben who has expressed nothing but interest and support of the work I conducted during my time at CEVT.

Ola Löseth, Gothenburg, June 2022

List of Acronyms

Below is the list of acronyms that have been used throughout this thesis listed in alphabetical order:

ASHRAE	American Society of Heating, Refrigerating and Air-Conditioning Engineers
CEVT	China-Euro Vehicle Technology
CFD	Computational Fluid Dynamics
HVAC	Heating, Ventilation and Air-conditioning
RNG	Re-Normalization Group

Contents

List of Figures

List of Tables

1
Introduction

1.1 Background

In recent times, modern man has become increasingly dependent on vehicle transport to meet the simple demands of life. For many people, the easiest way to get to and from work, to bring home essentials from the grocery store or to get to the doctor's office is to use ones car.

The modern reliance on the car and on the internal combustion engine that powers the car has had considerable consequences for the planet we inhabit. The internal combustion engine is usually powered by the combustion of hydrocarbons. The result is large emissions of pollutants that contribute to global warming. Due to the problems of global warming, considerable research efforts have been made to provide green alternatives to combustion engines.

The growing pressure from society to reduce greenhouse gas emissions has led to an increase in the demand for electrified transport systems. Although electric vehicles do not release emissions while driving, many new challenges must be overcome if electric vehicles are to replace conventional gasoline or diesel cars. One challenge is the difficulty of having a driving range that is comparable to that of combustion engine cars, while still having an acceptable level of passenger comfort. Since electric motors generate less heat than a combustion engine, climatizing a cabin in cold ambient conditions is very energy intensive for electric vehicles[2]. As a result, the driving range of the electric vehicle is greatly reduced.

Since a large fraction of the energy use in an electric vehicle goes into the climatization of the cabin, the focus of this thesis project will be to evaluate this process. This will be done using thermal comfort modeling to assess cabin climate and explore possibilities to improve energy efficiency. Additionally, development of the cabin simulation model itself will be another area of focus. The development of the cabin simulation model will be conducted to evaluate the possibility of increasing the flow field resolution within the cabin with the use of computational fluid dynamics (CFD) modeling.

1.2 Aim

The objective of this thesis is to develop and optimize models related to climate and energy for electromobility using thermal comfort models, 1D and 3D CFD modeling. The overall aim is to:

- Develop a cabin model that is accurate, yet feasible to integrate into a larger system model. This would involve a 3D-CFD simulation. Furthermore, a balance between running time and accuracy should be considered.
- Investigate areas in the system that could be further optimized with regard to energy usage, while also taking into account parameters such as thermal comfort and thermal sensation.
- Compare and develop existing cabin models to enhance their usability.

1.3 Limitations

Validation of the developed model is limited to comparison with the results of previously validated models, since there are no physical test data available for the vehicle used at the time of the thesis.

For the modeling of thermal comfort and sensation, the human representation is limited to 19 body segments, and the Berkeley Comfort Model is the comfort model used in this study. Furthermore, the software used for thermal comfort evaluation has a limit of 20000 elements for the structural mesh. This limits the resolution for the temperature fields, as well as the comfort model inside the thermal solver.

2
Theory

This section of the report will contain theoretical background on subjects such as fluid mechanics, heat transfer, and thermal comfort modeling, to the extent required to comprehend the topics of the thesis report.

2.1 Fluid mechanics

Fluid mechanics is known as the study of fluids; it can be fluids in motion, in which case it would be called fluid dynamics, or it can be fluids at rest, which is called fluid statics. A fluid can be either a gas or a liquid and since most objects are either a fluid or are surrounded by a fluid, the number of engineering applications related to fluid mechanics is enormous.

Although the fundamental properties and behavior of fluids have been well documented throughout time, there are several challenges when it comes to fluid mechanics. First, advanced geometries can make it extremely difficult to solve fluid-mechanical problems with the use of the basic governing equations of fluid mechanics. Therefore, most text book examples focus on basic geometries like flat plates or circular tubes. Second, the physical phenomenon called viscosity is one of the other great challenges of fluid mechanics. The most basic equations that describe fluid mechanics focus on idealized flow, which can neglect the effects of viscosity. In reality, however, no flow cases are ideal and even though there are more complete versions of the basic fluid mechanics equations as well as ways to approximate boundary layer flows, this can be incredibly difficult[3].

Viscosity has a destabilizing effect on all fluids that gives rise to another challenging phenomenon in fluid mechanics, namely turbulence. Turbulence is encountered in most flows, both in nature and industry, and it can be incredibly beneficial for industrial processes, since turbulence enhances both mass and heat transfer. Turbulence is, however, very difficult to give an exact definition of and, therefore, also challenging to predict or model. Cambridge researchers H. Tennekes and J.L. Lumley list the most important characteristics of turbulence as:

- Irregular. Turbulent flows are highly irregular and even considered chaotic or random. Furthermore, turbulence contains a wide range of length, time, and velocity scales. The turbulent motions are referred to as vortices or eddies.

- Diffusive. Turbulent diffusive transport is caused by chaotic motions in the flow. The diffusive effect allows for faster mixing of species and better transport of momentum and energy compared to that of molecular diffusion. The rates of these processes are also several magnitudes higher than those of molecular diffusion, making this a very important property in industrial applications.

- Instabilities at large Reynolds numbers. Turbulence is created because of instabilities in flows with a large Reynolds number. The Reynolds number is defined as the velocity, u, multiplied by the characteristic length, L, divided by the kinematic viscosity, ν. This can also be seen as the ratio between inertial and viscous forces within a fluid, which can be seen in the following equation. Furthermore, ρ represents the density and μ represents the dynamic viscosity of the fluid.

$$Re = \frac{uL}{\nu} = \frac{\rho u L}{\mu} \tag{2.1}$$

  At high Reynolds number, the term for inertial forces is far greater than that of the viscous forces. Since irregularities in flows are dampened by viscosity, flows show a greater tendency toward instability at high Reynolds numbers.

- Three-dimensional. All turbulent structures are three-dimensional, this is because two phenomena called vortex tilting and vortex stretching cannot occur in two dimensions. However, most modeling of turbulence in engineering implement methods that filter out 3D fluctuations.

- Dissipative. The phenomenon of turbulence is considered dissipative, this is because energy is dissipated or transported from the largest scale eddies to smaller scale eddies. This process continues until the smallest scale is reached, thereafter, energy is dissipated in the form of heat to the mean flow. This process is often referred to as the energy cascade. An illustration of the process can be seen in Figure 2.1 below.

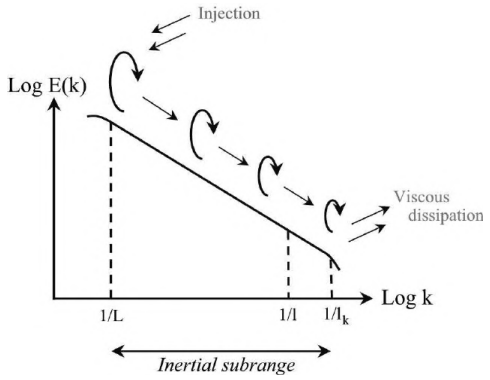

Figure 2.1: An illustration of the turbulent energy cascade. From [1]. CC BY-SA 4.0

- Continuous. Turbulence is considered a continuum phenomenon, since even the smallest scales of turbulent eddies are much larger than the molecular scales.

- Property of flows. Turbulence is a property of the flow, not the fluid. Every flow can become turbulent if the Reynolds number is high enough.

The challenges of fluid mechanics make it difficult to solve industrial problems with the use of just the governing equations for fluids. A more modern approach to solving these kinds of problem is to use a method known as Computational Fluid Dynamics, CFD, see Section 2.2. CFD makes use of models that have been validated through experimental studies. These models are then used to approximate numerical solutions to the problems at hand[4].

2.1.1 Governing equations

The governing equations for fluid flow and heat transfer discussed here are mathematical representations of the conservation laws of physics and are written on conservative form[5].

2.1.1.1 The continuity equation

The unsteady, three-dimensional continuity equation for compressible fluids can be written with vector notation in the following way.

$$\frac{\partial \rho}{\partial t} + div(\rho\,\mathbf{u}) = 0 \tag{2.2}$$

The first term describes the change of density with regard to time and the second term describes the net flow of mass, where $\mathbf{u}$ is a velocity vector with components u, v, and w that represent the velocity in the x-, y- and z-direction respectively.

For incompressible flow, the density ρ, is constant, and the continuity equation can be written as the following equation instead[5] .

$$div(\mathbf{u}) = 0 \tag{2.3}$$

2.1.1.2 The momentum equations

The momentum equations for fluid flow are derived from Newton's second law which states that the rate of change of momentum of a fluid particle equals the sum of forces acting on that particle. For unsteady, three-dimensional, and compressible flows, the momentum equations are written as seen in Equations 2.4-2.6.

$$x\text{-momentum} \qquad \frac{\partial(\rho u)}{\partial t} + div(\rho\, u\, \mathbf{u}) = -\frac{\partial P}{\partial x} + div(\mu\, grad\, u) + S_{Mx} \tag{2.4}$$

$$y\text{-momentum} \qquad \frac{\partial(\rho v)}{\partial t} + div(\rho\, v\, \mathbf{u}) = -\frac{\partial P}{\partial y} + div(\mu\, grad\, v) + S_{My} \tag{2.5}$$

$$z\text{-momentum} \qquad \frac{\partial(\rho w)}{\partial t} + div(\rho\, w\, \mathbf{u}) = -\frac{\partial P}{\partial z} + div(\mu\, grad\, w) + S_{Mz} \tag{2.6}$$

The first term represents how the momentum changes with respect to time. The second term represents the convective transport of momentum in the fluid. The third term is a pressure gradient. The fourth represents the diffusive transport of momentum, and the last term is a source term that contains body forces such as gravity or centrifugal force[5].

2.1.1.3 The energy equation

The energy equation is derived from the first law of thermodynamics which states that the rate of change of energy in a fluid particle is equal to the rate of work done on the particle plus the rate of heat addition on the fluid particle. This can be expressed as an equation for the internal energy, i, as seen in Equation 2.7 below.

$$\frac{\partial(\rho i)}{\partial t} + div(\rho i \mathbf{u}) = -P\, div\, \mathbf{u} + div(k\, grad\, T) + \Phi + S_i \tag{2.7}$$

Where Φ represents a dissipation function, T represents temperature, k represents thermal conductivity and S_i is a source term for the internal energy[5].

2.2 CFD

Traditional engineering modeling is often based on empirical or semi-empirical models that have been developed over time based on engineers' experience. These models work very well in systems or processes where conditions are known. However, empirical models can provide unreliable results for new processes where all conditions may not be known.

Product development and designing new equipment is a difficult task that has previously relied heavily on engineering judgment and down-scaled models. This has proven to be an expensive and time-consuming process. A more modern approach to the problems that arise in product development and research is to use a method

called computational fluid dynamics, or CFD for short. CFD is a numerical simulation method that allows the user to study and analyze the properties of the flow, combined with mass and heat transfer[4].

2.2.1 Meshing

When solving the flow inside of a geometric domain with the use of CFD, the domain first needs to be divided into smaller segments to form a grid of non-overlapping subsets of the domain. These smaller subsets are commonly known as control volumes, cells, or elements. Together they form a mesh grid over the domain, this is what is referred to as the mesh.

As the flow characteristics are computed by solving the governing flow equations in each cell, the quality of the solution is strongly related to the number of cells in the mesh. In general, a finer mesh resolution is needed where there are large variations of the flow properties, and a coarser mesh resolution can be applied where there are small variations. The result of a finer mesh resolution is both a higher accuracy of the flow solution and a higher computational cost due to the large number of computations that are performed in the cells. Due to the trade-off between accuracy and computational time and power, the meshing process in CFD is of great importance[5].

As seen in Equations 2.4 through 2.6, the governing equations for momentum transport are of non-linear characteristic. Hence, the discretization of the computational domain is of immense importance. To ensure accurate results, an analysis of the mesh grid should be performed to ensure that numerical diffusion will not occur as a result of poor mesh quality. The aspect ratio and the skewness of the mesh cells are common parameters analyzed that can ensure adequate mesh quality[4] .

2.2.2 Flow field mapping

When CFD results are desired for varying conditions in a certain computational domain, a method known as flow field mapping can be suitable. Instead of solving the transient flow directly, which can be very difficult, steady state solutions for different flow conditions can be used. The results from the steady state solutions can then be interpolated between to replicate transient flow. The result of this is both less computational power and less simulation time, while the accuracy of the flow solution remains high.

Flow field maps can be obtained by running steady state simulations in a 3D-CFD software and then exporting the data as a CFD-map. This function is available in most commercial CFD-softwares and makes it possible to use steady state solutions to emulate transient behavior, similarly to how look-up tables are used.

2.3 Heat transfer

Whenever a temperature difference exists within a medium or between media, heat transfer must occur. Heat transfer is defined as thermal energy in transit due to a spatial temperature difference, and is divided into three different modes[6].

2.3.1 Thermal conduction

The process of thermal conduction can be described as the transfer of energy from the more energetic particles of a substance to the less energetic particles of the same substance, due to the interactions between them.

The energy contained in molecules is related to the random translational motion, as well as the rotational and vibrational motions of the molecule. The collision of molecules results in an increase in temperature and consequently higher temperatures are directly related to higher molecular energies.

For example, a car door is being considered. It has heated air inside the door and colder air outside the door. This means that a temperature gradient will exist through the solid, and as a result the particles in the door that are located closer to the heated air will contain more energy than the particles which are located closer to the colder outside air. When molecular particles collide, as they constantly do inside the medium, the higher energy particle will transfer some energy to the lower energy particle. Therefore, when a temperature gradient exists, as in the case described, conductive heat transfer must exist in the direction of decreasing temperature. The thermal conduction process can take place in solids as well as in liquids and gases, where the main difference between them is the spacing of the molecules inside the medium.

All modes of heat transfer have equations that quantify the rate of heat transfer. These can be used to calculate the amount of energy that is being transferred per unit time. For thermal conduction, this equation is called *Fourier's law*. In one dimension, Fourier's law is expressed as the following equation.

$$q''_x = -k\frac{dT}{dx} \tag{2.8}$$

Where q''_x is the heat transfer rate in the x-direction, per unit area. Where the area is perpendicular to the direction of the heat transfer. The heat flux, q'', has the unit $[W/m^2]$[6].

2.3.2 Thermal convection

Thermal convection is comprised of two separate processes. The first process is energy transfer caused by random molecular motion, also called diffusion, while the second process is energy transfer caused by the bulk of the fluid, otherwise known as advection.

An example of thermal convection is being considered. A fluid in motion and a surface have different temperatures, where the surface has a higher temperature than the fluid flowing over the surface. The surface velocity u_s is equal to zero and gradually increases with the distance from the surface to the free flow velocity u_∞. This transition region is known as the boundary layer. The same phenomenon can be observed for temperatures. On the surface, a temperature of T_s can be observed, and with increasing distance from the surface, the temperature will change until the temperature of the free flow, T_∞ is reached. This region where the temperature change occurs is known as a thermal boundary layer. Since the temperature in the case of the example is higher on the surface, $T_s > T_\infty$, convective heat transfer will take place from the surface to the surrounding fluid.

As mentioned above, convective heat transfer is supported by both molecular diffusion and advection. Since the velocity is low close to the surface, this region is dominated by diffusive heat transfer. Similarly, further away from the surface where the flow velocity is higher, advection is the dominant force of convection.

Similar to Fourier's law that is used to quantify the rate of heat transfer for conductive processes, there is an equation that is used to calculate the rate of convective heat transfer, Equation 2.9 below is known as *Newton's law of cooling*.

$$q'' = h(T_s - T_\infty) \tag{2.9}$$

In the expression above, q'' represents the convective heat flux and has the unit $[W/m^2]$, h represents the convective heat transfer coefficient with the unit $[W/m^2 \cdot K]$ and T_s and T_∞ represent the surface and free flow temperatures, respectively[6].

2.3.3 Thermal radiation

The third and last mode of heat transfer is thermal radiation. Thermal radiation is defined as energy that is being emitted by matter that has a temperature larger than zero kelvin. The energy transported by thermal radiation is in the form of electromagnetic waves.

The energy that is emitted from a medium is derived from the thermal energy bound in the matter. The rate at which energy is released per unit area, (W/m^2), is known as its emissive power, E. The emissive power of ideal radiators, or blackbodies, can be calculated using *Stefan-Boltzmann law*, expressed in Equation 2.10.

$$E_b = \sigma T_s^4 \tag{2.10}$$

Here, E_b, is the emissive power of a blackbody, T_s, is the surface temperature of the matter and σ is the Stefan-Boltzmann constant. Instead, the expression for the emissive power of a real surface is expressed as in Equation 2.11, where ε is a material property called emissivity that can range between 0 and 1 and describes how efficiently a surface can emit energy relative to an ideal radiator.

$$E = \varepsilon \sigma T_s^4 \tag{2.11}$$

Radiation may also occur on a surface from its surroundings; this can be the case with sources such as the Sun, for example. In this case, the amount of energy that is being emitted from the source onto the surface is known as irradiation, G. Furthermore, a portion of the energy irradiated on the surface is absorbed by the material, thereby also increasing its thermal energy. The property of the material that determines the amount of energy absorbed by the material is known as the absorptivity, α.

Similar to the other modes of heat transfer, the net rate of radiation heat transfer per unit area may be calculated from the following equation.

$$q''_{rad} = \frac{q}{A} = \varepsilon E_b T_s - \alpha G = \varepsilon\sigma(T_s^4 - T_{sur}^4) \tag{2.12}$$

The expression in Equation 2.12 calculates the difference between the thermal energy emitted and the thermal energy absorbed by the surface[6].

2.4 Climate/comfort models

Modern tools make it possible to quantify thermal comfort with the help of mathematical models rather than by performing empirical tests. This opens up new opportunities in which cabin climatization can be optimized with respect to energy consumption. While this modeling opportunity is great, it is also very complex, and for the sake of the comprehension of this thesis, a differentiation of thermal comfort and thermal sensation has to be made.

2.4.1 Thermal sensation

The concept of thermal sensation is best explained by whether a feeling of warmth or chill is experienced when, for example, entering a vehicle cabin. If the surrounding environment is hot and the cabin has a lower temperature, the thermal sensation perceived by the body will be some degree of coldness. However, if the scenario is the opposite and the surrounding environment is cold while the cabin temperature is warmer, the thermal sensation experienced by the body will be some degree of warmth/heat.

The human body can feel several degrees of thermal sensation due to the thermoreceptors in the skin[7]. The different thermal sensations experienced by the body are cold, cool, indifference, warmth, and hot, ordered from low to high[7]. Since different parts of the body may experience different thermal sensations, this needs to be considered when designing, for example, a vehicle. Therefore, modeling of local thermal sensation has been applied in this thesis work.

When considering the example of the vehicle cabin, transient and non-uniform conditions will be experienced. Sitting in a hot car and then starting the ventilation system to lower the temperature is an example of this. The temperature will never be truly uniform and will change over time, and this is also true for most real-world examples[7].

2.4.2 Thermal comfort

The sensation known as thermal comfort is a subjective feeling experienced by the body based on the environmental properties surrounding the body. ASHRAE, which is the American Society of Heating, Refrigerating and Air-Conditioning Engineers, has published several papers that cover topics related to heating, cooling and thermal comfort.

In one of their publications, ASHRAE describes thermal comfort as the state of mind that expresses satisfaction with the thermal environment[8]. Furthermore, they state that the feeling of thermal comfort is highly subjective and that the environmental conditions required for comfort are not the same for everyone. However, since extensive empirical testing has been conducted within the subject, enough statistical data is available to define conditions that a specified percentage of occupants perceive as thermally comfortable. Furthermore, it is statistically shown that the six main properties that determine the thermal comfort of an individual are:

1. Metabolic rate
2. Clothing insulation
3. Air temperature
4. Radiant temperature
5. Air speed
6. Humidity

All of the aforementioned properties may vary with time, and because of this, a transient modeling approach would be the most accurate, precisely as for thermal sensation.

2.4.3 The Berkeley Comfort Model

While there are many models that can predict both thermal sensation and thermal comfort, the main benefit with the Berkeley Comfort Model is that it can be used for non-uniform environments as well as under transient conditions[7]. This allows the user to create simulation environments that emulate real-world scenarios more accurately.

The Berkeley Comfort Model[7] is a mathematical model that quantifies the perception of thermal properties by the human body using the temperatures of the core and skin. The model is capable of predicting both thermal comfort and thermal sensation for individual parts of the body and for the human body as a whole.

The model was developed by performing a multitude of tests on human subjects in a controlled environment. A non-uniform and transient environment was created by observing individual body parts until they reached a steady state. While the surface and core temperature of the body were measured, subjects answered questions regarding thermal comfort and thermal sensation throughout the tests to establish an adequate data set. A similar set of tests were carried out inside a wind tunnel to

emulate different air conditioning settings. These tests were performed for 19 individual parts of the body. The same type of test was also performed for the whole body[7].

The data obtained from these extensive tests were then used to develop mathematical models that describe local thermal sensation, local thermal comfort, overall thermal sensation and overall thermal comfort, with numerical values ranging from -4 to 4. The value -4 corresponds to the coldest sensation or lowest comfort value, and the value 4 corresponds to the hottest sensation or highest level of comfort in the Berkeley comfort model. These models have also been implemented in sophisticated softwares such as TAITherm, which allows the user to simulate the thermal comfort and sensation perceived by thermal manikins placed in different environments[7]. [1]

2.4.3.1 Model equations

The mathematical expression used to calculate the local thermal sensation in each of the 19 body segments is a function of the core and skin temperature. The expression is shown in Equation 2.13 below.

$$S_{Local} = 4(\frac{2}{1 + e^{-C1(T_{skin,local} - T_{skin,local,set})}} - 1) \tag{2.13}$$

In this expression, $T_{skin,local}$ is the skin temperature in the local body segment, see Figure 3.3, $T_{skin,local,set}$ is the skin temperature where the sensation value would be neutral, or zero, and $C1$ is a coefficient that varies for the different segments of the body.

The expression used to quantify local thermal comfort is more complex and is written as Equation 2.14.

$$C_{Local} = (\frac{C1 + C2So}{e^{5(Sl + C3So)} + 1} + C4 + C5So)(Sl + C3So) + C6 + C71|So^{-}| + C72|So^{+}| \tag{2.14}$$

In Equation 2.14 the constants $C1, C2, C3, C4, C5, C6, C71$ & $C72$ are coefficients that must be determined for each of the individual body segments; for information on how these are defined, refer to Human Thermal Sensation and Comfort in Transient and Non-Uniform Thermal Environments by Hui Zhang[7]. Furthermore, Sl & So are local and general sensations, respectively. Moreover, So^{+} is referring to hot overall sensations while So^{-} refers to cold overall sensations.

[1] Information about TAITherm can be found in Section 3.2

The overall thermal sensation is expressed as a weighted average, where the different body segments have varying weighing factors. The expression can be seen in Equation 2.15.

$$S_{overall} = \frac{\Sigma \text{weight}_i S_{local,i}}{\Sigma \text{weight}_i} \tag{2.15}$$

Finally, the quantified value of the overall thermal comfort is calculated using two rules that are expressed in the following way:

1. Overall comfort is the average of the two minimum thermal comfort votes (the two lowest local comfort values), unless rule 2 applies.
2. If the following two criteria are met:
   - The second lowest local comfort vote is less than -2.5
   - The subject has some control over their thermal environment or the thermal conditions are transient

   then the overall thermal comfort is the average of the two minimum votes and the maximum comfort vote.

3
Method

The aim of this thesis is to develop the current cabin simulation methodology used by CEVT and to further utilize the analysis of thermal comfort models to optimize energy usage. Furthermore, the results obtained from the developed method are to be analyzed in order to evaluate the methodology. The workflow developed for the method and the software used for each step throughout this project is shown in Figure 3.1. To protect sensitive information about the vehicle used in this project, all figures depicting the geometry have been replaced with that of another vehicle.

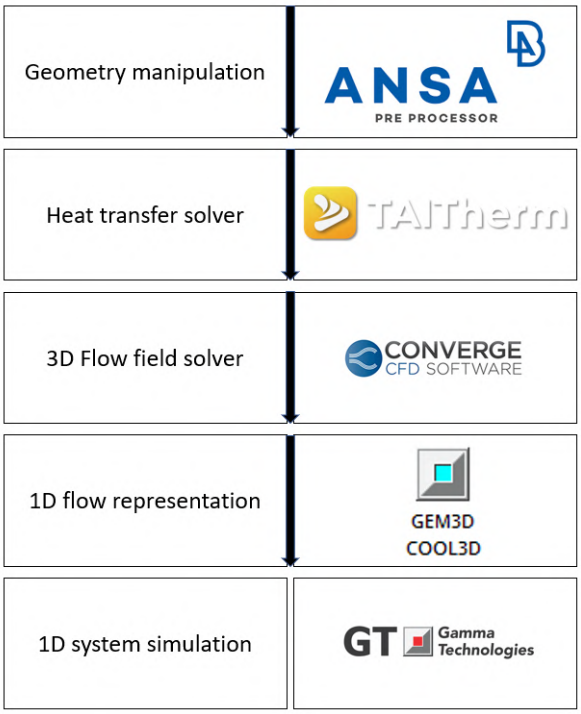

Figure 3.1: A graphical representation of the thesis work flow.

As seen in Figure 3.1, the first course of action was to perform geometry manipulation and generate a mathematically representative structural mesh of the cabin in the software ANSA. The generated structural mesh could then be used to prepare the thermal solver TAITherm[9] to obtain a heat map of the environment. Thereafter, the 3D-CFD model was prepared and simulated in Converge, producing results containing fluid properties such as velocity profiles and local convective heat transfer coefficients. This could then be converted into a 1D representation of the flow using GEM3D. Lastly, all of the previous steps were combined and utilized in

order to create a 1D simulation system environment in the software GT-SUITE. The main difference between this method and the one previously used is that a 3D-CFD simulation of the cabin volume has been introduced to more accurately depict the flow characteristics inside the cabin.

3.1 ANSA

To perform the simulation, the geometry had to first be imported into a software called ANSA. ANSA is a tool that enables the user to make changes to geometry models and to create mesh grids suitable for numerical simulations.

When the CAD geometry of the vehicle cabin had been imported into ANSA, geometrical errors first had to be addressed so that a waterproof mesh could be exported once all the manipulation had been finished. Geometrical errors can take the form of intersecting surfaces, non-connected surfaces, or gaps in the geometry, for instance. Second, it can be beneficial to perform actions to simplify the geometry. This is done to decrease the total number of mesh elements on the geometry surface to speed up the simulation time. A highly complex geometry can also cause an increased difficulty for the software to generate a mesh with a sufficient quality standard; hence, geometry simplification was utilized to more easily obtain an adequate mesh quality.

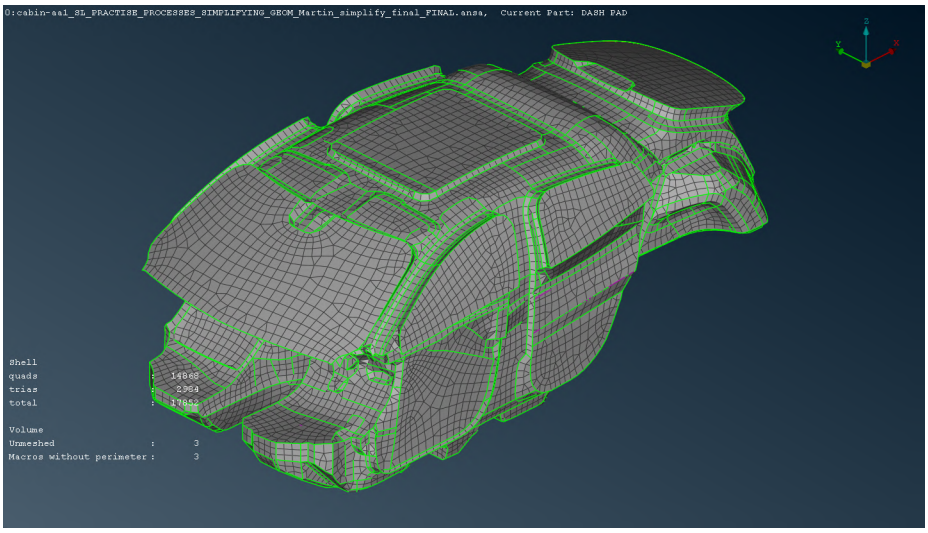

Figure 3.2: A computational mesh for the cabin geometry.

In ANSA, there are tools implemented to optimize the mesh for the purpose of the model application. In this case, the purpose of the model was CFD. Therefore, the launch option dedicated to CFD was selected. The results of this can be seen in Figure 3.2, where the mesh is constructed of both tetrahedrons and quadrahedrons. The mixing of mesh elements was implemented to obtain the optimal numerical accuracy when the mesh was used later in the numerical simulations. Sub-optimal mesh quality could induce numerical diffusion in the calculation and the quality of

the result would decrease as a consequence.

In Figure 3.2, a completed cabin mesh can be visualized. This particular mesh has a total number of mesh elements of about 18000. For this project, the total element count was kept below 20000 since that was a limitation for the comfort model implemented in the thermal solver TAITherm. Furthermore, all geometries that were to be used in TAITherm had to be meshed; this includes both the cabin geometry and the thermal manikin geometry.

3.2 TAITherm

TAITherm is a numerical simulation tool that can calculate steady-state and transient heat distributions over complex geometries. During simulation, the software calculates thermal conduction, thermal convection, and thermal radiation to produce a temperature map of the geometry model imported into the software.

To allow simulation of the thermal behavior of the cabin, the mesh constructed in ANSA first had to be imported into TAITherm. Subsequently, the cabin model had to be further adjusted by defining boundary conditions and material properties. Finally, this had to be completed for the entire cabin model before the thermal simulation could be run.

To accurately predict thermal conduction in the cabin, the material properties of all cabin surfaces had to be defined, including all individual layers of each cabin surface. The properties of most materials were obtained from the material property library integrated in TAITherm, but some values had to be manually defined as well. Once all surfaces had the correct material properties, the convection boundary conditions could be applied. For surfaces that are in contact with the air volume inside the cabin, a co-simulation condition was applied for both the convection coefficient and the velocity magnitude of the flow. This was done because the purpose of this model was to later be coupled with a 3D-CFD solution[1]. For surfaces that were not in direct contact with cabin air, Dirichlet conditions were applied, as no 3D-CFD was performed for the fluid surrounding these surfaces.

3.2.1 Human manikin model

In order to accurately model the comfort level of a driver or passengers inside the cabin, an extension of TAITherm was utilized. This extension allows for the introduction of thermal manikins that can be placed inside the cabin to replicate humans. The manikins are segmented into 19 different body segments according to the Berkeley comfort model[2]. The human modeling extension includes the Berkeley comfort model, which is used to solve the bio-heat transfer on the 3D-human model.

[1] See Section 3.5
[2] See section 2.4.3

This allows the model to accurately mimic the characteristic physics of humans. In Figure 3.3 the segmentation of the meshed thermal manikin can be seen.

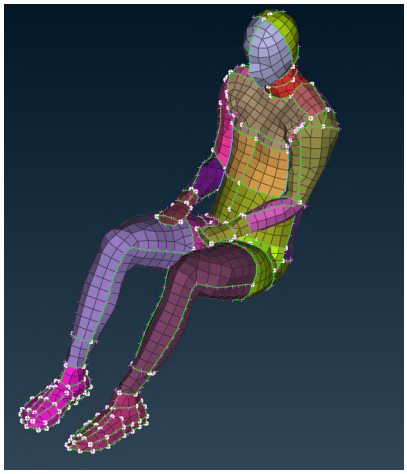

Figure 3.3: A computational mesh for the thermal manikin where the different colors represent the different body segments.

To further improve the accuracy of the human model, physiological properties were used for each layer of the human. This includes bone, fat, muscle, and skin. In addition to physiological layers, clothing layers were also applied to the model to ensure realistic behavior. The clothes used on the manikin were taken from a TAITherm database that includes a large selection of clothes that have properties such as density, thermal conductivity, and thermal resistance predefined. Moreover, it is also possible to introduce custom materials or clothes directly into the database if that is more suitable for the application. This was used in the simulation case with respect to winter clothing.[3]

Before inserting the human manikin into the cabin, the assumption was applied that the manikin was pre-conditioned to an average room temperature. This was done to emulate a scenario in which the driver was indoors prior to entering the vehicle. Therefore, the manikin was introduced into an environment with an ambient temperature of 22°C in order to create a reference state for the manikin.

3.3 Converge

To solve the flow characteristics inside the cabin, the 3D-CFD solver Converge was used. Converge is a CFD software that can be used to calculate the flow properties of fluids in complex geometries[10]. The use of 3D-CFD is advantageous for this application, since the flow data obtained from the solution can be coupled directly to the thermal solver TAITherm. Furthermore, there is a version of Converge that is adapted specifically for GT-SUITE which allows for the CFD solution to be easily implemented in the rest of the simulation system.

[3]See section 3.6.2

3.3.1 Converge Studio

When using Converge, the initial course of action was to export a binary STL file from the ANSA geometry. This file could then be imported directly into Converge Studio, where an automatic meshing tool generates a new mesh for the geometry. It is not possible to use the mesh generated in ANSA since Converge requires a structured mesh. Therefore, a new mesh was generated. Similarly to the ANSA procedure[4], geometrical errors caused by the meshing had to be resolved inside Converge Studio before any flow simulations could be run.

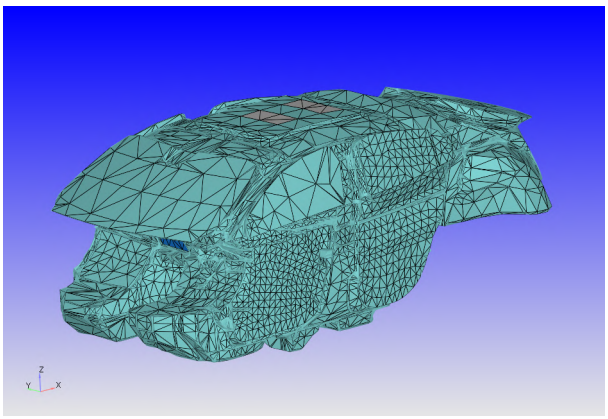

Figure 3.4: An example visualization of the Converge Studio environment.

The next step was to divide the geometry surfaces into key features, which is necessary to simulate the flow. These features include the different inlets and outlets for the flow, as well as the wall features. In Figure 3.4 a visual representation of the aforementioned features can be seen, where the turquoise cells are wall features and the grey and blue cells are two different vent inlets. This new and adjusted surface geometry could then be exported as a data file that could later be implemented in the GT-Converge simulation environment.

3.3.2 GT-Converge

After the geometry manipulation had been completed inside of Converge Studio, the CFD solver had to be set up. This was done directly in GT-SUITE by utilizing the native template CFDGTCONVERGE. This template allows the user to define all the boundary conditions necessary before running the GT-Converge CFD solver.

3.3.2.1 Fluid and flow properties

To run the different GT-converge simulations, the fluid and flow properties had to be defined. These properties included the composition of the fluid species, initial temperatures, volume flow rate, initial turbulent kinetic energy, initial turbulent dissipation, and initial pressure. In Table 3.1 below, the boundary conditions used for the heating simulations are specified.

[4]See section 3.1

Table 3.1: Fluid and flow properties used in a cabin heat-up case.

	Heating (-18 °C)
Initial ambient temperature [°C]	-18
Fluid species composition (mass fraction) [%]	O_2 (23) N_2 (77)
Total inlet volume flow rate [m^3/h]	216
Initial turbulent kinetic energy [m^2/s^2]	1
Initial turbulent dissipation [m^2/s^3]	120
Initial pressure [atm]	1

3.3.2.2 Boundary conditions

The boundaries described in 3.3.1 were defined as either velocity inlets, pressure outlets, or walls. For the velocity inlets, the different velocity components were defined as well as the turbulence length scale and intensity. Finally, for the velocity inlets, the inflow species and the inflow temperature were defined. For pressure outlets, a pressure boundary condition was established and, as for walls, thermal boundary conditions and near-wall treatment were defined.

3.3.2.3 Turbulence model

To capture important features of the flow, a fitting turbulence model had to be selected. Since the flow inside the cabin contains swirls and re-circulation, the selection of the RNG $k-\varepsilon$ model was regarded suitable. This was the model of choice since it handles swirls and re-circulation better than, for example, the standard $k-\varepsilon$ model[4]. When analyzing the flow fields received from GT-Converge in the post-processing software ParaView, it could be seen that substantial amount of re-circulation and swirling was actually occurring, and therefore the RNG $k-\varepsilon$ model was deemed a good choice for the application of this cabin simulation.

3.3.3 Flow field mapping

In order to solve the heat transfer in the cabin while maintaining high flow resolution and moderate computational costs, flow field mapping was used, as described in Section 2.2.2. Data from the GT-Converge CFD simulation were used to create a "map" for that specific flow configuration. The same procedure was then repeated with different volume flows. This was done because flow field mapping is a technique that is best utilized when CFD results are available for several different flow configurations.

3D-CFD is generally expensive with regard to computational power and is therefore not very suitable for coupling directly to the system environment. Instead, the data saved in the flow field maps could be used in the simulation system. As a result, relatively high flow field resolutions could be obtained in the GT-SUITE 1D solver, which uses significantly less computational power than a coupled 3D-CFD solver. The result of this method is both higher accuracy for the solution and a lower computational cost.

The quantities included in the flow field maps were the velocity, geometry of the inlets, outlets, fluid volume, and wall boundaries, pressure, heat flux, turbulent viscosity, and temperatures.

3.3.3.1 CFD map study

The cabin environment considered in this project is of a transient nature and will have a varying volume flow of air entering the cabin. Because of this, several CFD maps, computed with different volume flows, were included in the model.

Since a large system simulation is very time consuming, the CFD-map study was conducted on a simulation system containing only the cabin and HVAC modules. This smaller system was significantly faster and much more suitable for this map study. The exclusion of the other models that are included in the larger system environment was considered acceptable in the case of this study, since the dependency of the different systems are not of that significant importance. The results obtained from this study can be seen in Section 4.1.

3.4 GEM3D

To accurately model a 3D fluid domain within a 1D GT-SUITE system, GEM3D can be a useful tool. Flow and geometry data acquired from GT-Converge can be used directly to create an accurate 1D environment, representative of the 3D fluid domain simulated in GT-Converge.

For the model setup considered in this thesis, temperature sensors were placed close to the relative position of the head and feet of the four different seat positions. This was done to allow the possibility of later evaluating the temperatures at these positions, in addition to the thermal comfort and thermal sensation of the thermal manikin inside the cabin. In Figure 3.5a the cabin environment as well as the inlets and outlets can be seen, where the features in the back of the cabin are the outlets.

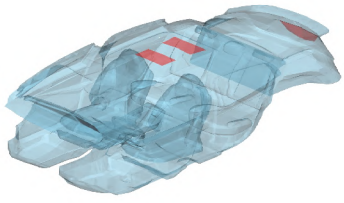

(a) The cabin volume inside GEM3D.

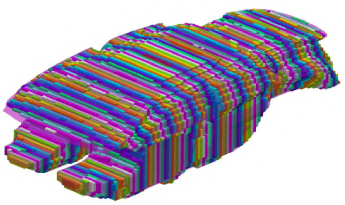

(b) The discretized cabin volume in GEM3D.

Figure 3.5: Graphical representations of the work performed in GEM3D.

Once all desired geometries and sensors were included in the GEM3D model, a volume discretization of the cabin volume could be made and thereafter it could be

exported as an external GT-subassembly. This made it possible to directly implement the model in a 1D GT-SUITE system. For this project, a cell volume with a width, length, and height of 30 mm was used to discretize the cabin volume. The discretized GEM3D cabin volume can be seen in Figure 3.5b above.

3.5 GT-SUITE

To implement the different models in order to build an accurate representation of the cabin in a system environment, the multiphysics software GT-SUITE was used.

3.5.1 GT-ISE

GT-ISE, the graphical interface for GT-SUITE, was used to combine the different simulation models and create a simulation system. This was done using built-in templates as well as the external subassembly exported from GEM3D. In addition, the simulation model created for the cabin environment could be further integrated into a system environment which is representative of the entire thermal system of the electric vehicle. This is beneficial since it allows us to see how the rest of the system affects the cabin environment and vice versa.

3.5.1.1 Cabin subassembly

To create a simulation environment representative of the vehicle cabin, a cabin subassembly was created inside GT-SUITE. In order to do this, the model exported from GEM3D, pipes, ducts, and different monitoring signals were introduced to the subassembly. In addition, boundary conditions such as the volume flow rate and the inflow temperature were defined. Lastly, a native GT-SUITE template was introduced to the model that allowed GT-SUITE to communicate with the previously created TAITherm model, and thereby couple them. Furthermore, the mapped CFD data were included in the template to allow the software to interpolate between the maps based on the volume flow entering through the ventilation system.

3.5.1.2 System simulation environment

Once a functioning cabin subassembly was created, the model could be further integrated into a larger system environment. This larger model is a simulation model that couples all the different components and systems included in the electric vehicle thermal system into a single GT-SUITE model. The purpose and benefit of the system environment is that the dependencies of the different components and subsystems can easily be monitored in the post-processing tool GT-POST[5].

3.5.1.3 Integration of cabin model

In order to integrate the cabin subassembly into the larger system environment, several actions had to be considered. These actions were mainly related to how

[5]See Section 3.5.2

communication and integration of GT-SUITE subassemblies are resolved in the current GT-SUITE version[6].

Second, since the purpose of the cabin subassembly is to run in a transient setting, the choice of using multiple flow field maps was implemented in the model. This is because the system has a transient behavior with a variable volume flow fed to the cabin from the condenser. For cases like this, GT-SUITE needs several flow field maps to select from and to interpolate between to obtain adequate accuracy. Furthermore, the template used for the coupling between the CFD data and the cabin subassembly does not have the ability to extrapolate values. Because of this, flow field maps with a suitable range of volume flows should be included if adequate accuracy is to be obtained. Moreover, the software, GT-SUITE, utilizes linear interpolation, but as physical behavior often is nonlinear, the total number of flow field maps included in the model should also be considered and evaluated.

To allow GT-SUITE to select which maps to utilize and interpolate between when integrating the cabin model into the larger system environment, two wireless signals were used. These signals contained the information on the vent configuration that the system was to use, as well as the volume flow fed to the cabin. Based on this, the software then interpolated between the two maps that were closest to the signal values, to emulate a transient flow scenario, and then impose the flow on the cabin model.

Another factor that was important to consider when integrating the cabin model into the larger system environment is the communication interval used in the coupling between GT-SUITE and TAITherm. From the different simulation runs performed in this project, it was found that the communication interval was important for the stability of the simulations. Therefore, the communication interval was continuously lowered throughout this project, in order to obtain better simulation stability.

3.5.2 GT-POST

GT-POST is the post-processing software integrated in GT-SUITE. It can be used to monitor simulation runs as well as to create plots and graphs that can be used to evaluate the results obtained from the simulation.

In Figure 3.6 a monitor that was used during a simulation can be seen showing the temperature at one of the sensor positions in the cabin. Monitors such as the one visible in Figure 3.6 can be used to assess whether the solution is converging or not; as seen in the figure, the temperature does not fluctuate at the end of the simulation and can be considered to be converging. However, this may not be the case for all properties. Because of this, several monitors that contain results that are critical for the purpose of the simulation should be evaluated before considering a converged solution, air flows, and residuals among them.

[6] v2021.3 is the software release used for this project

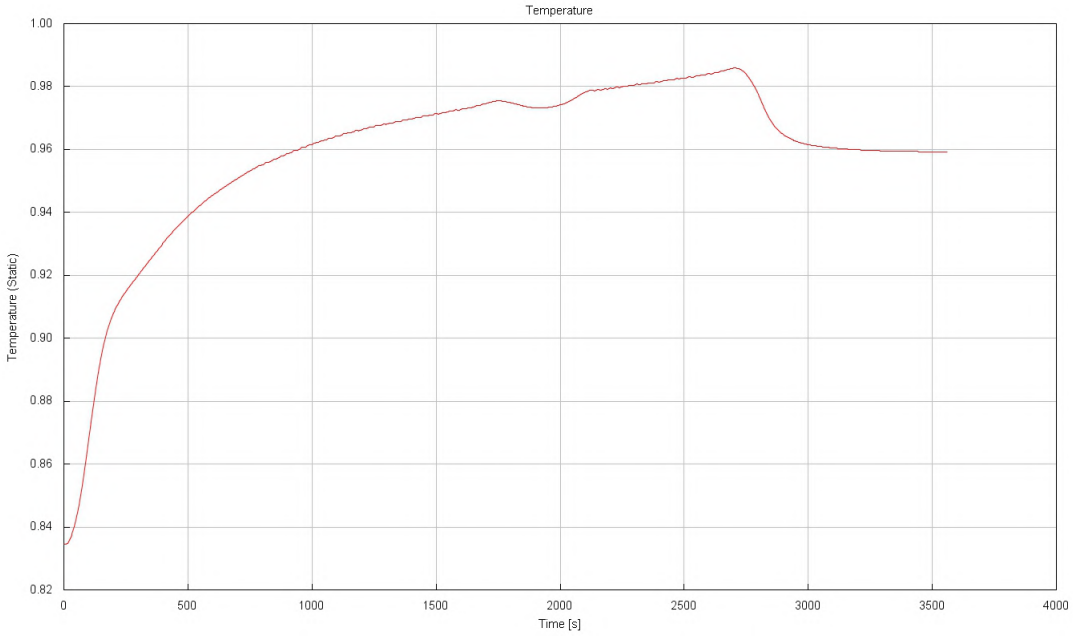

Figure 3.6: An example visualization of a GT-POST monitoring plot.

Furthermore, GT-POST was used to create transient 3D representations containing information such as the wall or fluid temperatures inside the cabin. The transient plots make it possible to analyze the properties during certain varying driving conditions and for the entire driving duration. An example of this type of graphical post-processing can be seen in Figure 3.7 below, where the thermal comfort of the thermal manikin can be seen for three different time steps.

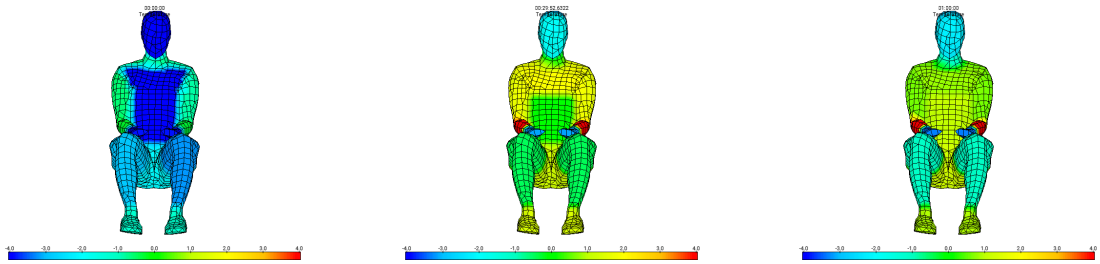

(a) t=0 **(b)** t=30 min **(c)** t=60 min

Figure 3.7: Transient thermal comfort results for a thermal manikin located in an environment with an ambient temperature of 20 °C. The scale used is that of the Berkeley Comfort Model; see Section 2.4.3.

3.6 Simulation cases

Two different scenarios for the cabin were to be considered and therefore also simulated. The main case for this thesis was the so-called heating scenario. Heating scenarios are meant to emulate cold ambient conditions when the cabin must be heated to be comfortable for the driver and potential passengers occupying the cabin.

In addition to the main scenario mentioned above, another case was considered as part of an energy optimization study. This case was supposed to evaluate how energy consumption could be reduced during heating if climatization was adjusted based on the clothing worn by the driver. If the cabin climatization temperature can be reduced while still achieving adequate thermal comfort levels for the cabin occupants, this shows great opportunities to increase the energy efficiency of the vehicle.

3.6.1 Heating case

The cabin heating simulation was set up using both the cabin subassembly and the system environment, which were detailed in Section 3.5. Furthermore, a TAITherm model was created with the methodology described in Section 3.2. The ambient temperature was set at -18 °C and it was assumed that the cabin surfaces were soaked to the same temperature. The velocity profile of the vehicle drive cycle can be seen in Figure 3.8. It is assumed that the vehicle is driving at a velocity of 50 km/h for the first 30 minutes of the simulation; then it accelerates and drives at a velocity of 100 km/h for the next 30 minutes before decelerating to stand still and idle for the last 10 minutes of the simulation.

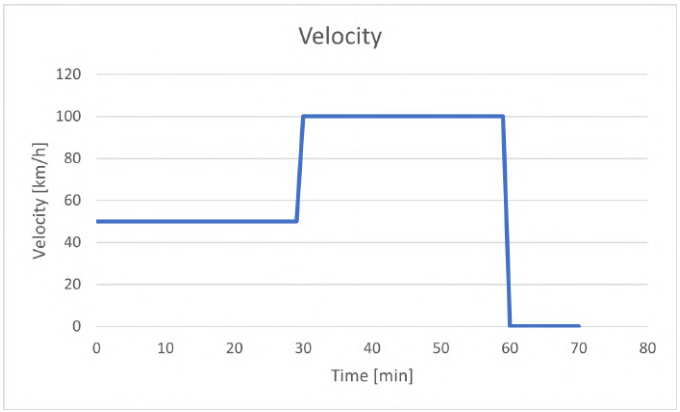

Figure 3.8: The driving cycle velocity profile used in the simulation.

Furthermore, the climate control model used in the system environment to control cabin climatization was set to target a cabin temperature of 22 °C. The clothing specified for the thermal manikin used to evaluate thermal comfort inside the cabin is listed in Table 3.2 and the thermal properties of the clothing are listed in Table 3.3.

Table 3.2: The clothing of the thermal manikin used in the reference heating case.

Head	Hair	
Torso	Long sleeve shirt with collar	
Legs	Straight, long denim trousers	
Feet	Calf length athletic socks	Soft-soled athletic shoes

Table 3.3: The thermal properties of the clothing defined on the thermal manikin for the heating case.

	Thickness [mm]	Vertical evaporative resistance [m^2kPa/W]	Vertical thermal resistance [m^2K/W]
Hair	5	0.028	0.155
Long sleeve shirt with collar	2	0.0199	0.125
Straight, long demin trousers	2	0.0151	0.129
Soft-soled athletic shoes	1.2	0.052	0.222
Calf length athletic socks	1.5	0.042	0.066

3.6.2 Detection of winter clothes

As mentioned, a simulation case was run as part of this thesis that was supposed to predict how much energy could be saved when climatizing the cabin if winter clothing could be detected.

The simulation was set up with the same methodology as in the other case, using the same system environment and cabin subassembly. However, the TAITherm model had to be adjusted. This was done by defining winter clothing and adding these clothes to the thermal manikin[11][12]. The clothes used for this simulation can be seen in Table 3.4 below. After the clothes were defined, tests were conducted inside TAITherm to assess how different cabin temperatures would impact the thermal comfort and sensation of the thermal manikin seated in the driver seat. The thermal properties of the clothes used in the winter clothing case are depicted in Table 3.5.

Table 3.4: The clothing of the thermal manikin used in the winter clothing heating case.

Head		Hair		
Torso		Thermal underwear top	Long sleeve turtleneck	Down jacket
Legs		Thermal underwear bottoms	Straight, long denim trousers	
Feet		Calf length dress socks	Hard-soled street shoes	

Table 3.5: The thermal properties of the clothing defined on the thermal manikin for the winter clothing case.

	Thickness [mm]	Vertical evaporative resistance [m^2kPa/W]	Vertical thermal resistance [m^2K/W]
Hair	5	0.028	0.155
Down jacket	2	0.1148	0.418
Long sleeve turtleneck	2	0.0394	0.261
Thermal underwear top	1.2	0.0086	0.094
Straight, long denim trousers	2	0.0151	0.129
Thermal underwear bottoms	1.2	0.0076	0.08
Soft-soled athletic shoes	1.5	0.079	0.222
Calf length athletic socks	1.2	0.0417	0.075

To evaluate the thermal comfort of the driver at different temperatures, the dressed thermal manikin was placed in environments with different ambient temperatures for 60 minutes, and then the thermal comfort and sensation were analyzed to see how the environment was perceived. The conditions of the different environments, as well as the results of the tests, can be seen in Section 4.4.1. It should be noted that these climatization tests did not take into account the convective effect of the fans in the actual cabin environment and were only used to obtain approximate results.

Once an appropriate target temperature had been found from the tests, the climate control model inside the system environment could be adjusted so that the cabin was climatized to that target temperature. For the winter clothing case a target temperature of 18 °C was used.

4
Results and discussion

Throughout this thesis work, a new methodology has been examined that combines fluid dynamics and heat transfer in three dimensions with the simulation of a vehicle cabin in a system environment. The results obtained will be presented, analyzed, and discussed in the following section. The data displayed in the graphs have been normalized to preserve sensitive information about the vehicle used in this study.

4.1 CFD map study

As mentioned in Section 3.3.3.1 a study was conducted with the purpose of getting an understanding of how the simulation results are affected by varying the amount of flow field maps used. The results of that study will be presented here.

In Table 4.1, the different map configurations used in the study are depicted. In total, five different map configurations were tested. However, only four results are included in the results. The results obtained from the simulation that was run with a 2-map configuration, using 5% and 120% of the total volume flow, could not converge and was therefore not included. In the comparison of the cases, the 7-map configuration is used as a reference as it utilizes all available CFD data.

Table 4.1: The different map configurations, where the percentages are fractions of the total volume flow.

	5%	20%	40%	60%	80%	100%	120%
2 maps	◇						◇
2 maps		◇			◇		
3 maps	◇			◇			◇
5 maps	◇	◇		◇		◇	◇
7 maps	◇	◇	◇	◇	◇	◇	◇

In Figures 4.1 to 4.3 results are shown for the volume averaged temperature, the temperature at the head position of the driver, as well as the relative humidity at the head position of the driver. Due to instabilities at the end of the simulation duration, only the first 47 minutes of the data have been used in the analysis. Figure 4.1a shows the results for the duration of the whole simulation and Figure 4.1b shows the results for a part of the simulation. As seen in Figure 4.1a, all configurations except the one using 2 maps have quite similar results. Looking at the data in the zoomed in graph, seen in Figure 4.1b, it can be seen that the configurations using 3

and 5 maps slightly underestimate the temperature, while the 2-map configuration overestimates the temperature quite significantly compared to the results of the 7-map configuration.

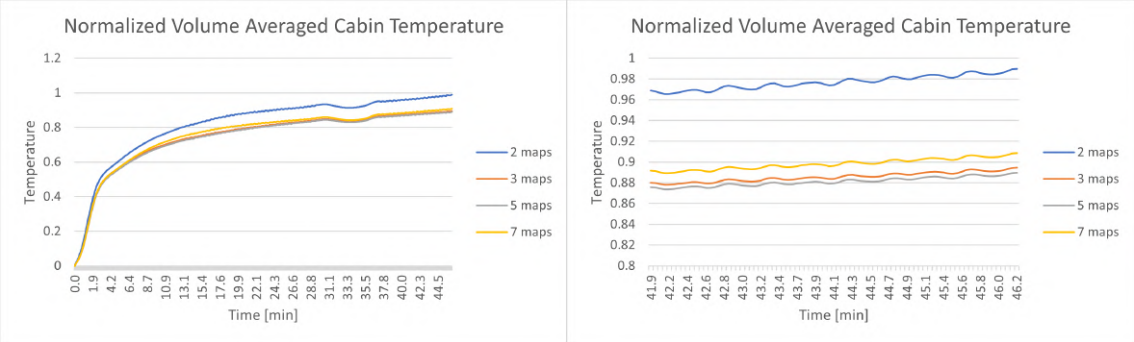

(a) Complete results. **(b)** Partial results.

Figure 4.1: Graphs showing the normalized volume averaged temperature in the cabin for the different map configurations.

Similar results are seen in Figure 4.2 where Figure 4.2a shows that the temperature results of the 2-map configuration are significantly higher than those of the remaining configurations. However, in Figure 4.2b it can be seen that the 5-map configuration slightly underestimates the solution, while the 3-map configuration slightly overestimates the solution compared to the results obtained from the 7-map configuration.

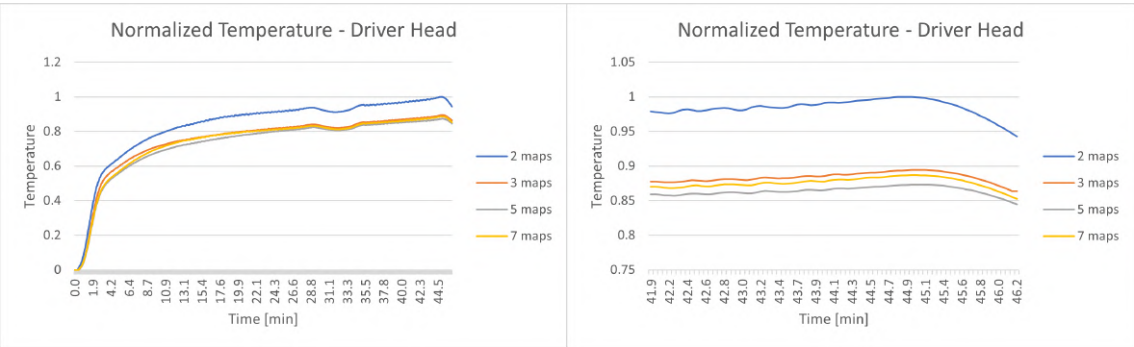

(a) Complete results. **(b)** Partial results.

Figure 4.2: Graphs showing the temperature at the head position of the driver.

In Figure 4.3 the relative humidity in the driver head position is presented for the different configurations. As seen in Figure 4.3a, all configurations are fairly similar, except for the solution for the 2-map configuration, which has significantly lower humidity than the others. In the zoomed in graph in Figure 4.3b, the same observation can be made. Moreover, it can be seen that the results from the 5-map configuration are slightly higher than those from the 7-map configuration. However, the results of the 3-map configuration are slightly lower than those of the 7-map configuration.

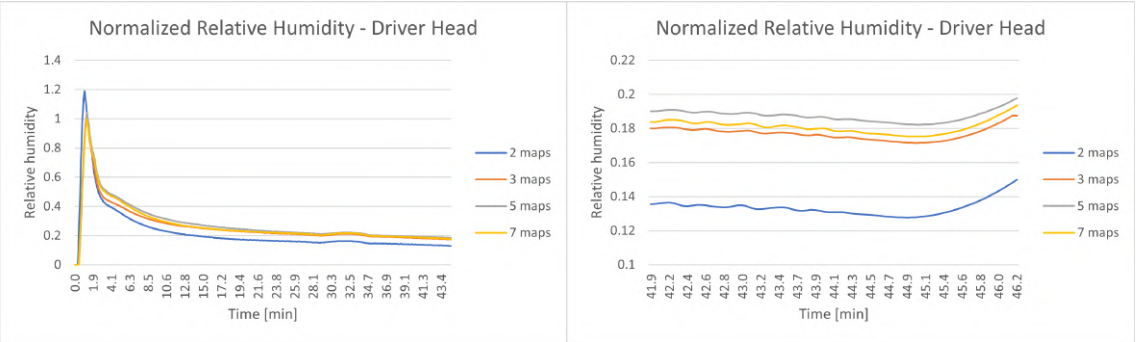

(a) Complete results. **(b)** Partial results.

Figure 4.3: Plots showing the relative humidity at the head position of the driver.

From the results presented, it is evident that there is a correlation between the simulation accuracy and the amount of flow field maps used in the simulation. Unfortunately, there are no physical test data available to validate which configuration is closest to reality. However, since the simulations in question have a transient characteristic, more maps should in theory be more accurate, since more flow field data are available for the software to interpolate between.

From this study it can be concluded that the results of the different configurations are quite similar to each other, except the 2-map configuration, which has significantly deviating results. This shows that the choice of configuration depends on how accurate results are required, as well as the amount of time available to generate flow field maps. For all simulations conducted in this thesis, the 7-map configuration was selected to obtain maximum accuracy with the available time.

4.2 Method development

A big part of this thesis project was to further develop an existing method used to model the cabin environment of an electric vehicle. The development was carried out by solving the cabin flow using 3D-CFD and then coupling the data obtained from the flow solution to the thermal solver. Subsequently, the new cabin model was integrated into a larger system simulation environment.

The introduction of 3D-CFD in the cabin model allowed the solver to utilize more realistic fluid properties than the previous method. Local velocity profiles and convective heat transfer coefficients further improved the accuracy of the heat transfer solver. This in turn also should improved the accuracy of the results obtained from the Berkeley Comfort Model.

Although the increased resolution of the flow field inside the cabin should result in more accurate results, the simulation time increased significantly as a result. Consequently, the increased simulation accuracy comes at the cost of a 1167% increase in simulation time. However, there are other factors that also impact the simulation time. The frequency with which the different post-processing results are saved is an

example of a contributing factor to the increase in simulation time, and the time steps used in the simulation is another one.

4.3 Heating case

The case referred to as the heating case in the report is the simulation case described in Section 3.6.1. For this case, the cabin is soaked at -18 °C and then heated to a target temperature of 22 °C. Furthermore, the thermal manikin is wearing the clothes seen in Table 3.2. The results obtained for this simulation case are presented in the following section.

4.3.1 System simulation - Heating case

Since the main focus of this thesis is thermal comfort, the results presented below are related to the thermal characteristics of the simulation environment. Moreover, both simulation setups use the driving cycle presented in Figure 3.8.

The impact of the heating procedure used in the simulations on driver thermal comfort is presented in Figures 4.4-4.6 below. It can be seen that the thermal comfort of the legs and torso increases moderately with time. However, the thermal comfort of the areas with exposed skin, i.e. the face and the hands, is decreasing with time. Furthermore, it can be seen that the overall thermal comfort of the thermal manikin is quite decent, with values reflecting neutral and good comfort on large sections of the body. Nevertheless, there are areas that experience slight discomfort as seen in the figures. As mentioned previously, these are mainly areas with exposed skin, but also the feet, which also experience slight discomfort. In the figures displayed below, the thermal manikin is seated in the cabin environment; however, only the manikin is visible since the thermal comfort and sensation are considered.

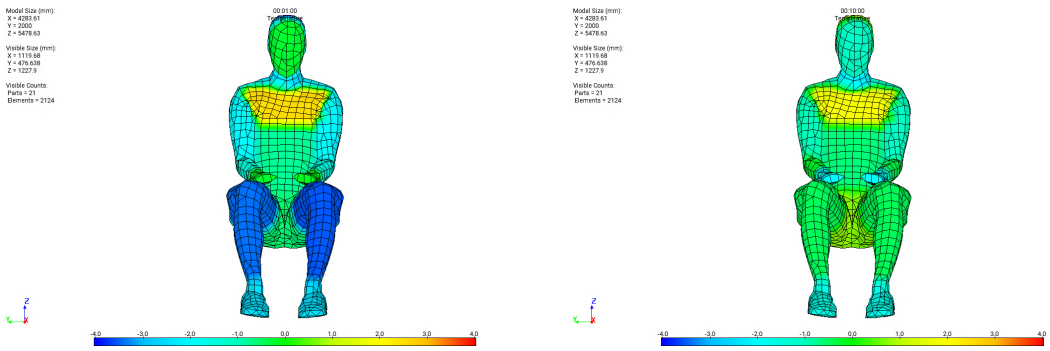

(a) Thermal comfort after 1 min. **(b)** Thermal comfort after 10 min.

Figure 4.4: Thermal comfort of the manikin in the heating case.

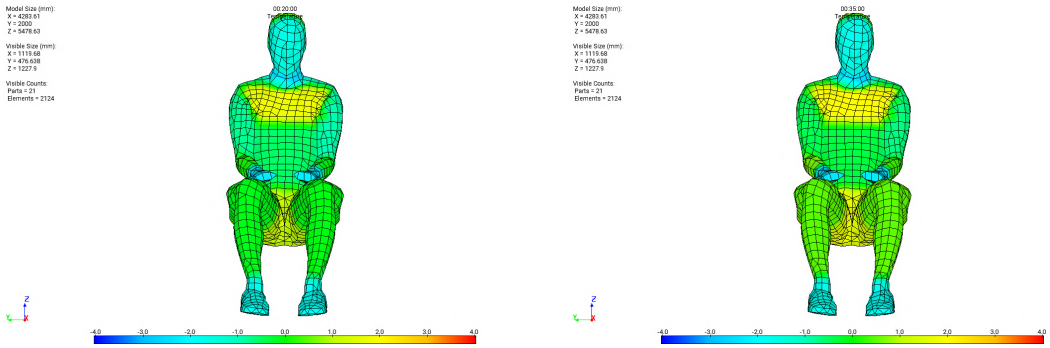

(a) Thermal comfort after 20 min. **(b)** Thermal comfort after 35 min.

Figure 4.5: Thermal comfort of the manikin in the heating case.

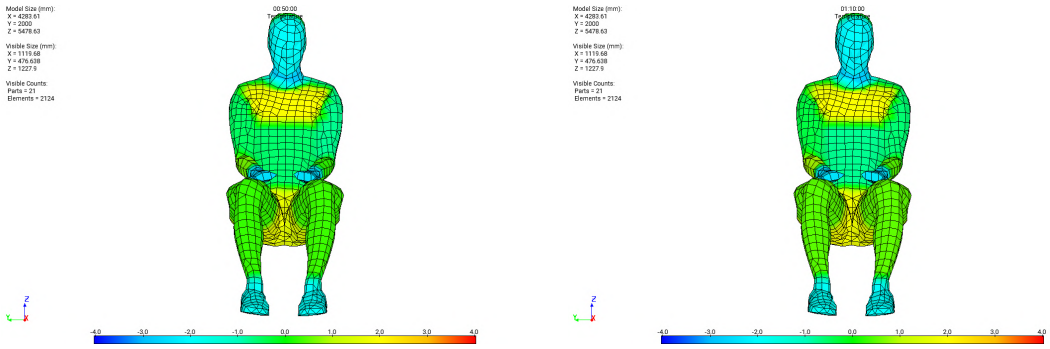

(a) Thermal comfort after 50 min. **(b)** Thermal comfort after 70 min.

Figure 4.6: Thermal comfort of the manikin in the heating case.

The perception of thermal sensation by the thermal manikin during the heating procedure is shown in Figures 4.7-4.9 below. From these figures, it is evident that the manikin experiences slight cold in most areas of the body throughout the duration of the simulation. However, as seen in Figures 4.4-4.6, this does not necessarily translate into discomfort in most areas of the body.

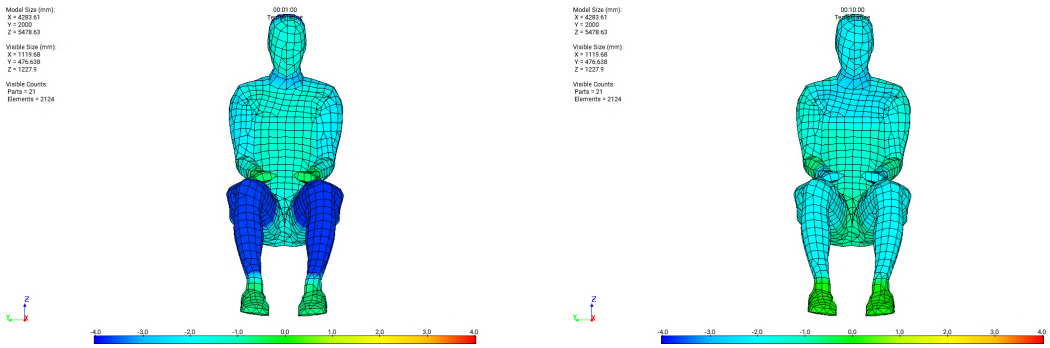

(a) Thermal sensation after 1 min. **(b)** Thermal sensation after 10 min.

Figure 4.7: Thermal sensation of the manikin in the heating case.

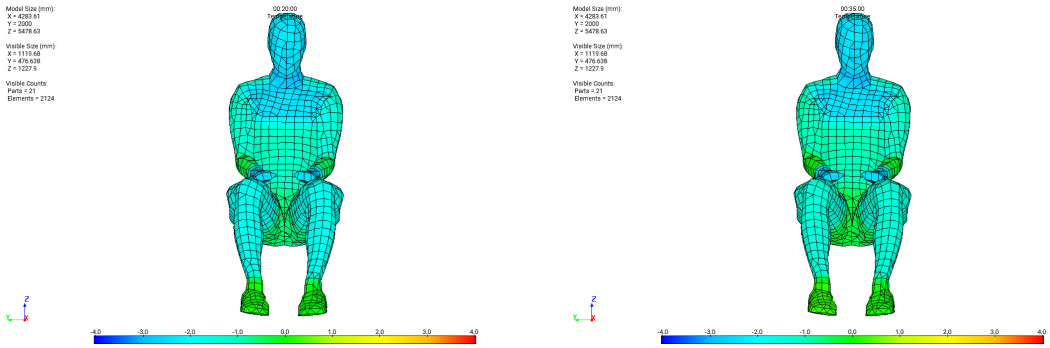

(a) Thermal sensation after 20 min. **(b)** Thermal sensation after 35 min.

Figure 4.8: Thermal sensation of the manikin in the heating case.

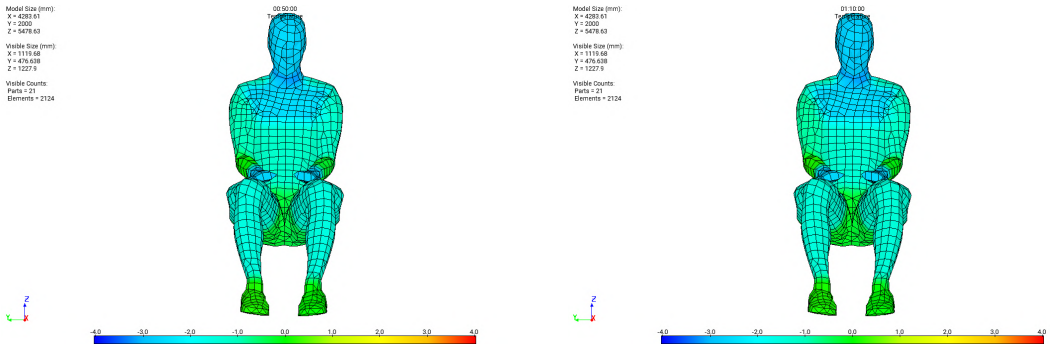

(a) Thermal sensation after 50 min. **(b)** Thermal sensation after 70 min.

Figure 4.9: Thermal sensation of the manikin in the heating case.

To compare the thermal results of the manikin between the heating case and the case of winter clothing, graphs representing the skin temperature in different body positions are included in Figures 4.10 and 4.11 below. From these graphs, it can be seen that the skin temperatures decrease rapidly during the beginning of the simulation. This is expected since the thermal manikin is pre-conditioned in an environment with an ambient temperature of 22°C while the cabin is soaked to a temperature of -18 °C. For the rest of the simulation duration, the change in skin temperature is quite moderate.

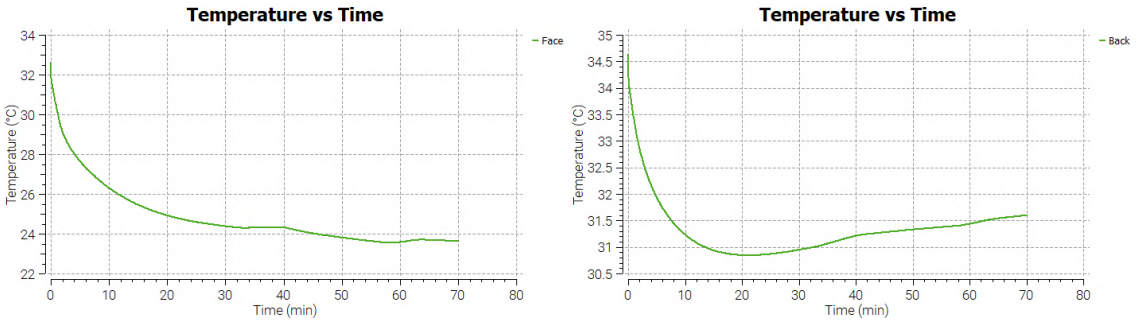

(a) Average skin temperature on the face. **(b)** Average skin temperature on the back.

Figure 4.10: Average skin temperature on the manikin.

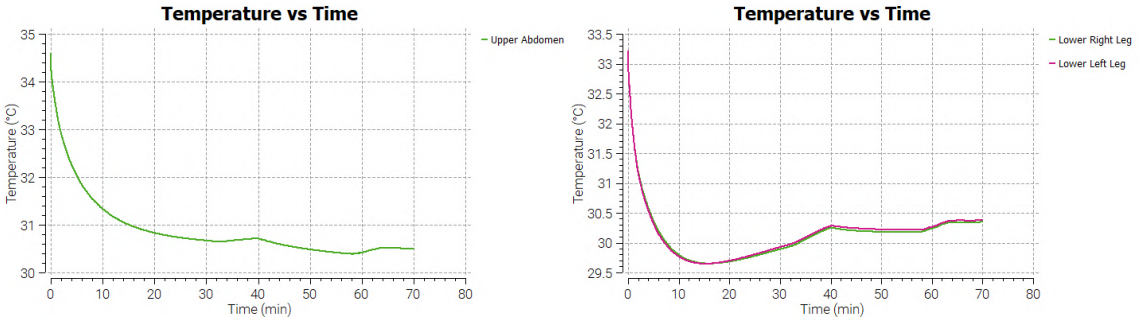

(a) Average skin temperature on the upper abdomen. **(b)** Average skin temperature on the lower legs.

Figure 4.11: Average skin temperature on the manikin.

Similarly to the graphs above, Figures 4.12 to 4.15 present the local thermal comfort on the face, back, upper abdomen, and lower legs.

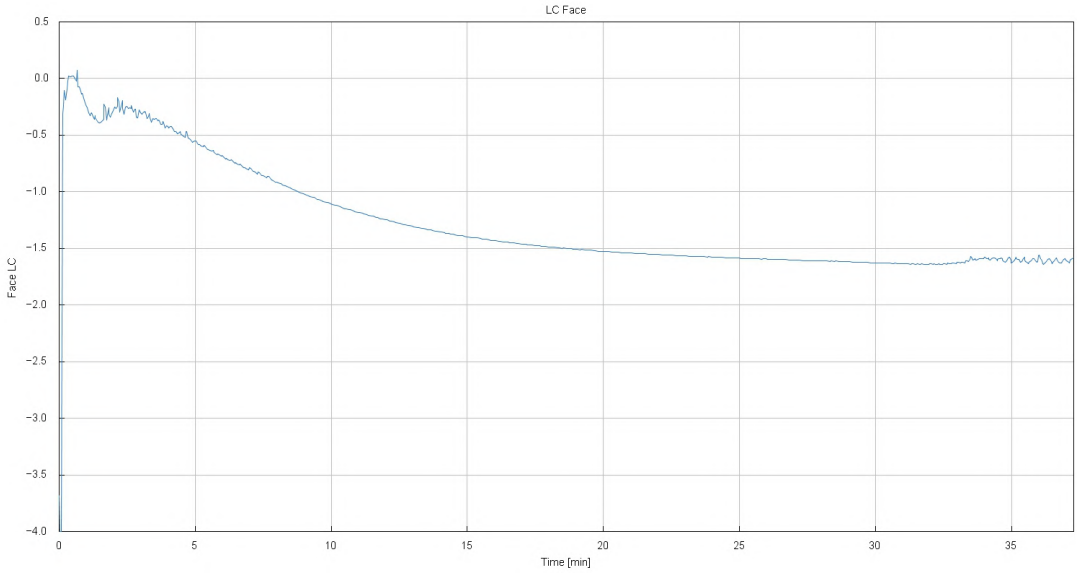

Figure 4.12: Thermal comfort on the face.

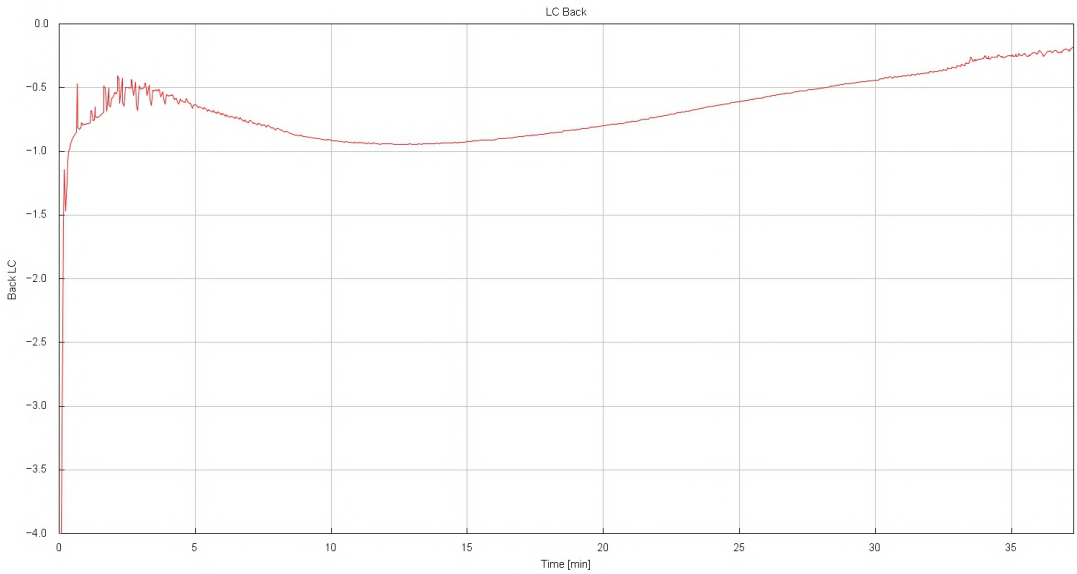

Figure 4.13: Thermal comfort on the back.

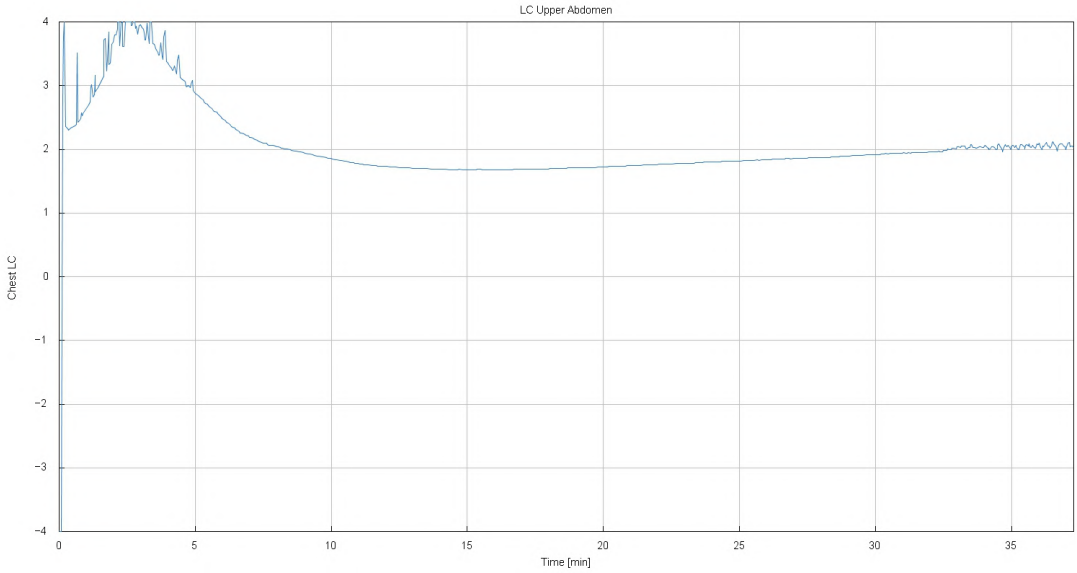

Figure 4.14: Thermal comfort on the upper abdomen.

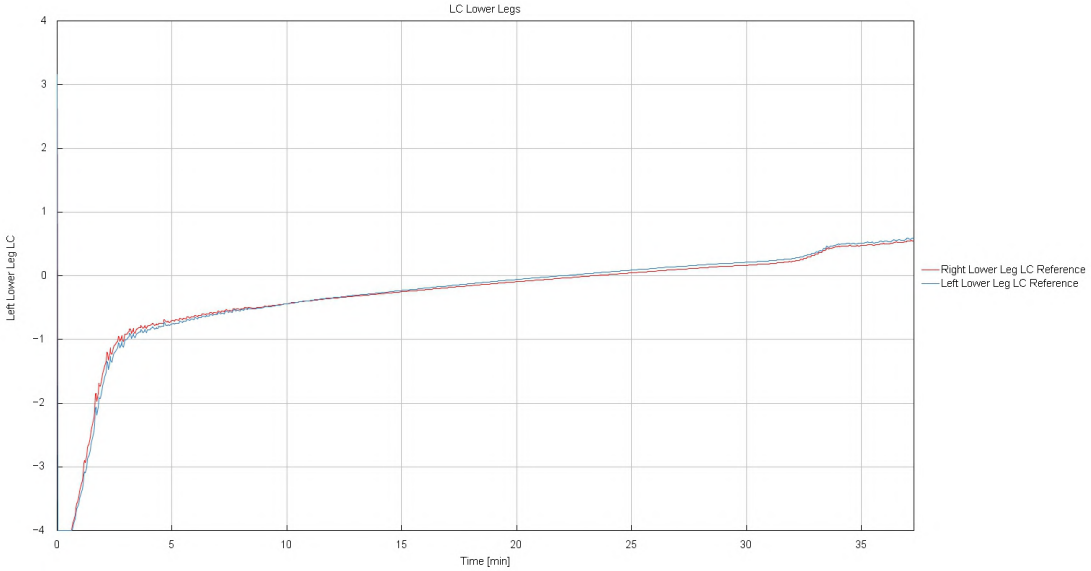

Figure 4.15: Thermal comfort on the lower legs.

Thermal comfort is seen to increase rapidly at the beginning of the climatization and then stay quite stable. This is true for the back, upper abdomen, and lower legs; however, the thermal comfort of the face decreases throughout the simulation. This may be the case because the face is without any clothing providing thermal insulation, as well as the neck and head which are located close to the face also have relatively low thermal insulation. Furthermore, the figures show that the thermal comfort perceived by the different body segments is quite spread out. The upper abdomen perceives relatively high values, while the back, face, and lower legs perceive lower values of thermal comfort.

The graphs seen in Figures 4.16 and 4.17 represent the properties of selected parts of the thermal system. In Figure 4.16 the condenser energy rate is visualized, as well as the auxiliary load of the thermal system. Furthermore, the average battery temperature and the volume averaged cabin temperature are presented in Figure 4.17.

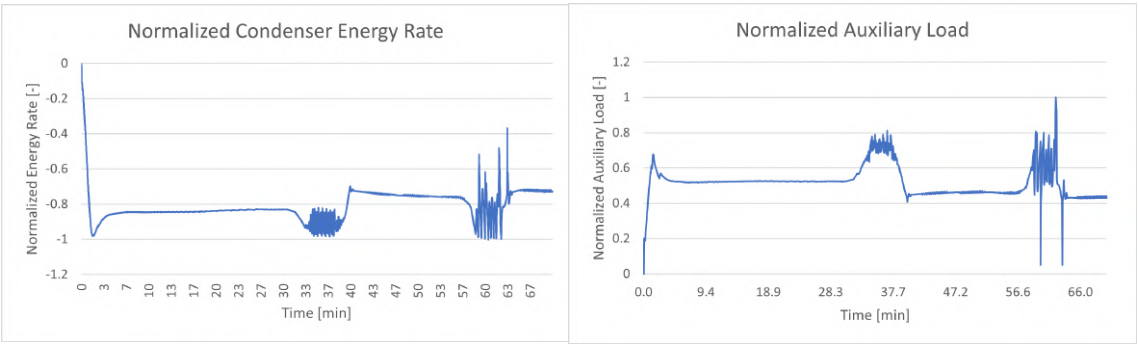

(a) Condenser energy rate.

(b) Auxiliary load of the system.

Figure 4.16: Performance of the thermal system.

From Figure 4.16a it can be seen that the condenser heat rate is uniform throughout

the duration of the simulation. However, after about 30 minutes, it can be seen that some instability is occurring before the energy rate decreases slightly. The same phenomenon can also be seen after about 60 minutes. This occurrence is due to the change in the velocity profile seen in Figure 3.8. The change in the driving cycle causes a reaction from the climate control model that adjusts the cabin climatization. As a result, slight instabilities can be seen in the condenser energy rate in Figure 4.16a. The auxiliary load of the thermal system, observed in Figure 4.16b, has similar characteristics. It is quite stable for the first 30 minutes, then it experiences slight instabilities before stabilizing again. The same happens after about 60 minutes as well, due to the change in the driving cycle discussed earlier.

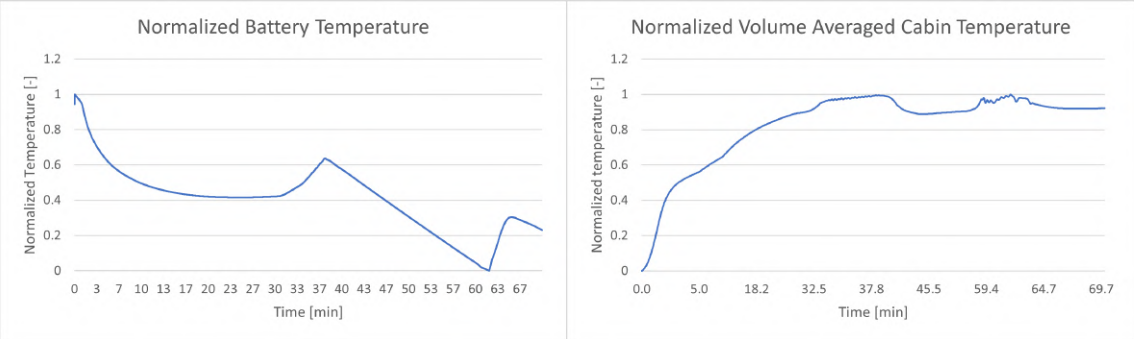

(a) Average battery temperature. **(b)** Volume averaged cabin temperature.

Figure 4.17: Temperature of system components.

In Figure 4.17a it can be seen that the average battery temperature decreases slightly at the start of the simulation; this is because an assumption that the battery is pre-conditioned has been applied as an initial condition. Apart from that, the same characteristics can be seen as in the previous figures, where changes correlate strongly with the driving cycle. This property is especially important in development of sustainable vehicles, as the temperature of the battery affects the rate of battery degradation. Moreover, a parameter that is incredibly important when considering thermal comfort is the cabin temperature. In Figure 4.17b, the normalized volume averaged cabin temperature is presented. It can be seen that the temperature increases during the entire first part of the driving cycle, and then it decreases slightly before increasing again for the last part of the cycle. It can also be observed that oscillations occur approximately as the driving cycle changes, precisely as for the other parameters discussed.

4.4 Detection of winter clothes

As mentioned in Section 3.6.2, one of the cases that were simulated in this thesis was a heating case in which the driver was wearing winter clothing. The purpose of this simulation was to evaluate whether a lower cabin temperature could be targeted while still achieving adequate thermal comfort for passengers. The results of said simulation could then show how much energy could be saved and potentially reallocated towards driving range as an example.

4.4.1 Climatization temperature tests

To evaluate how much the target cabin temperature could be lowered while still achieving acceptable thermal comfort for the driver, climatization tests were performed in GT-TAITherm. The results of these tests are presented in Figures 4.18-4.22 below. Furthermore, the thermal conditions for the different tests are presented in Table 4.2 below.

Table 4.2: Properties used for each of the tests conducted on the thermal manikin.

Case	1	2	3	4	5
Ambient temperature [°C]	10	12.5	15	17.5	20
Ambient relative humidity [%]	40	40	40	40	40

Looking at the results obtained from the 5 different climatization cases, it can be seen in Figure 4.18b that the driver perceives the environment as neither hot nor cold for test case 1. As a result of this, the comfort values experienced by the manikin are quite high. This is directly reflected in Figure 4.18a. When comparing the results of test case 1 with those of case 2 in Figures 4.19a and 4.19b, it can be seen that the results for the two cases are very similar, both in terms of thermal comfort and sensation. However, the main difference is that the comfort level in the hands has increased with increasing temperature and that the thermal comfort in the neck area has decreased slightly.

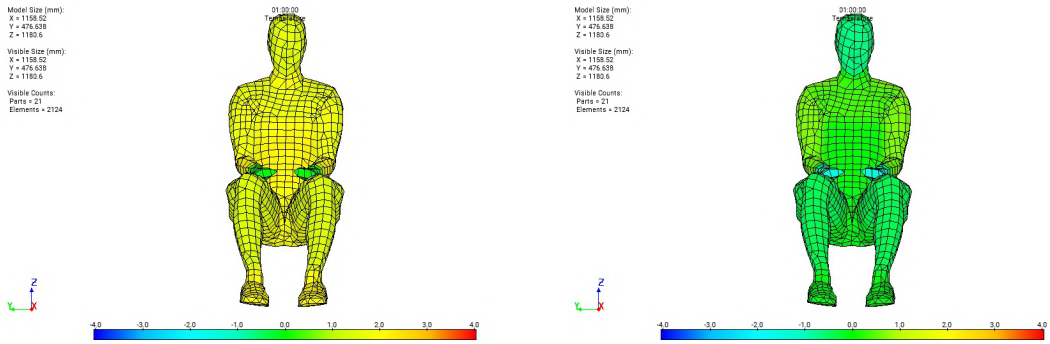

(a) Thermal comfort. **(b)** Thermal sensation.

Figure 4.18: Thermal comfort and sensation visualized on the thermal manikin for test case 1.

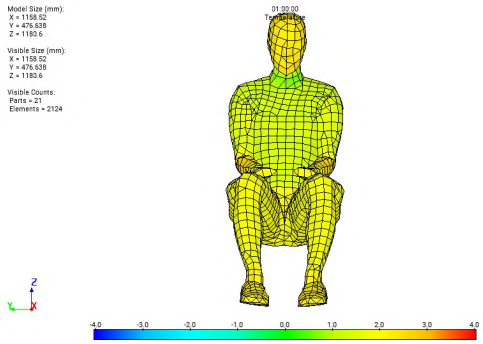

(a) Thermal comfort.

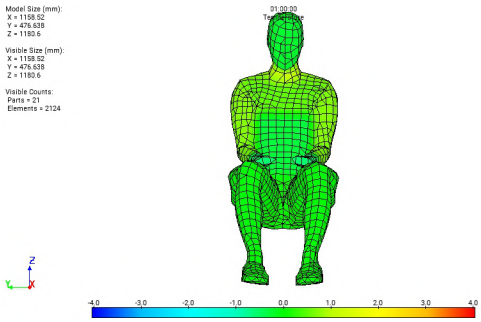

(b) Thermal sensation.

Figure 4.19: Thermal comfort and sensation visualized on the thermal manikin for test case 2.

When analyzing the results of cases 3 through 5, it becomes evident from the thermal sensation results in Figures 4.20b, 4.21b, and 4.22b, that the manikin begins to perceive the environment as hot in the areas of the head and hands. As a result of this, the thermal comfort values seen in Figures 4.20a, 4.21a and 4.22a are not as uniform as for the first two cases. Furthermore, it can be seen that increasing temperature slightly lowers the comfort value of both the upper and lower body, while the comfort of the head and hand areas is significantly lowered.

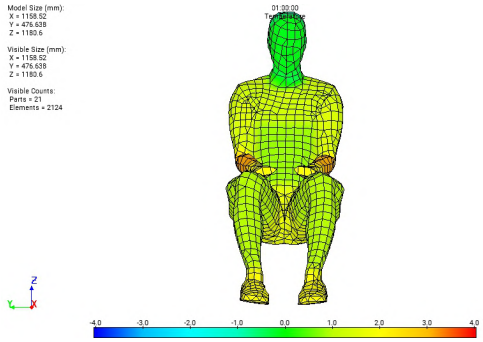

(a) Thermal comfort.

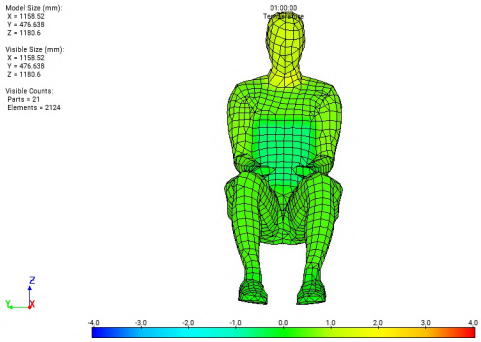

(b) Thermal sensation.

Figure 4.20: Thermal comfort and sensation plotted on the thermal manikin for test case 3.

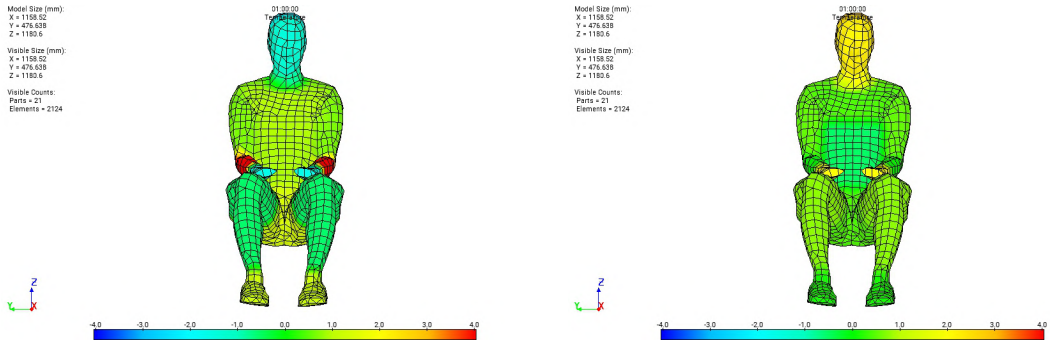

(a) Thermal comfort. **(b)** Thermal sensation.

Figure 4.21: Thermal comfort and sensation plotted on the thermal manikin for test case 4.

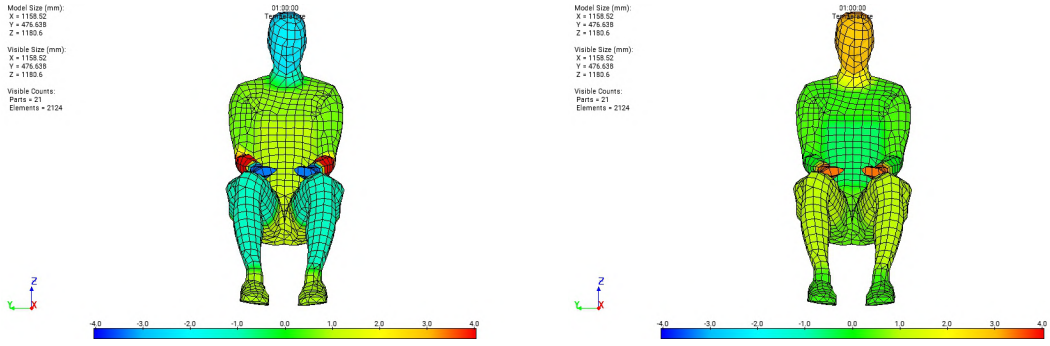

(a) Thermal comfort. **(b)** Thermal sensation.

Figure 4.22: Thermal comfort and sensation plotted on the thermal manikin for test case 5.

Based on the results obtained from these tests, it was found that the temperature used in test case 2 gave the most satisfactory results with respect to thermal comfort. Therefore, it was originally used as a temperature request for the climate control model in the system simulation environment for the winter clothing case. However, due to the low cabin temperature target, the climate control model had quite unsteady behavior. The unstable behavior caused the results obtained from the simulation to be poor. Furthermore, it seemed unrealistic that areas with exposed skin did not experience lower thermal comfort values in the tests with colder ambient temperatures, and because of this, a simulation with a more conservative target temperature of 18 °C was run instead. The results obtained will be presented in the following section.

4.5 System simulation - winter clothing case

In this section the results obtained from the simulation setup described in Section 3.6.2 will be presented and discussed. Precisely as for the heating case, the velocity profile and vent configuration described in Section 4.3 was used.

The thermal comfort of the manikin is presented for the same time steps in Figures 4.23-4.25. Apart from the results seen in Figure 4.23a, the thermal comfort is quite high for all sections of the body. However, after 1 minute, it can be seen that the thermal comfort perceived on the legs and head is quite low. This is to be expected, as the cabin is cold at the start. For the rest of the simulation, the thermal comfort results are significantly improved as a result of the continuous cabin climatization.

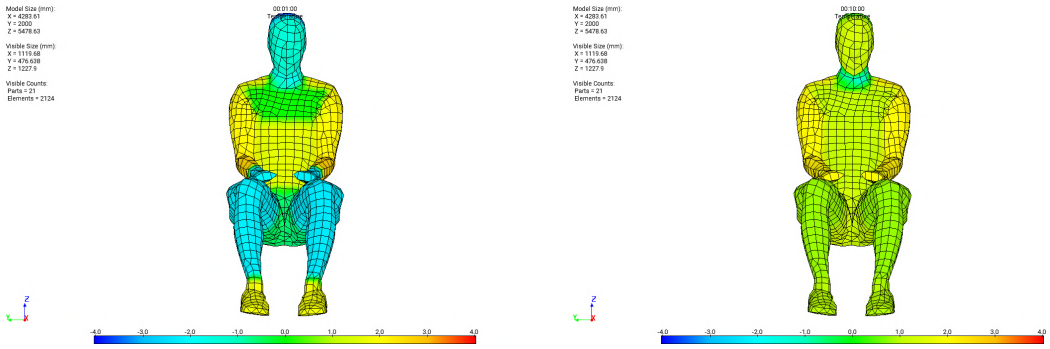

(a) Thermal comfort after 1 min. **(b)** Thermal comfort after 10 min.

Figure 4.23: Thermal comfort of the manikin in the winter clothing case.

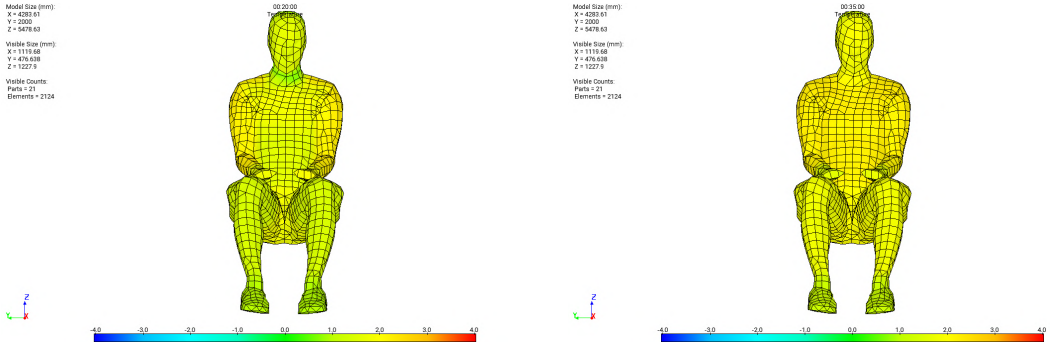

(a) Thermal comfort after 20 min. **(b)** Thermal comfort after 35 min.

Figure 4.24: Thermal comfort of the manikin in the winter clothing case.

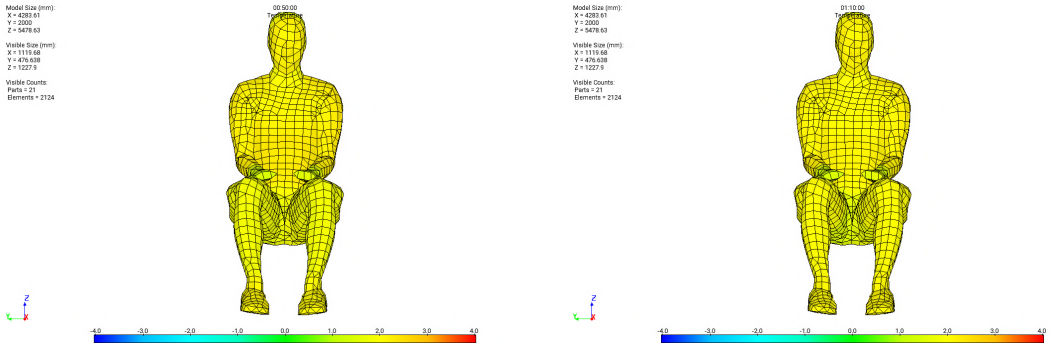

(a) Thermal comfort after 50 min. **(b)** Thermal comfort after 70 min.

Figure 4.25: Thermal comfort of the manikin in the winter clothing case.

The results of thermal comfort are a direct reflection of the results of thermal sensation portrayed in Figures 4.26-4.28. As seen in Figure 4.26a, the legs perceive some cold, while the head is rather hot. As a result, the thermal comfort seen in Figure 4.23a is quite low for both the legs and the head. For the rest of the thermal sensation results, it can be observed that the values gradually go toward neutral. In turn, the overall thermal comfort is very good for the majority of the simulation duration.

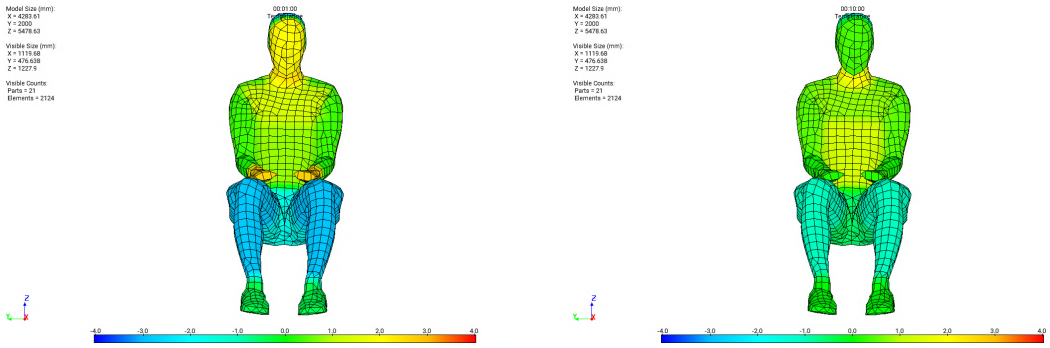

(a) Thermal sensation after 1 min. **(b)** Thermal sensation after 10 min.

Figure 4.26: Thermal sensation of the manikin in the winter clothing case.

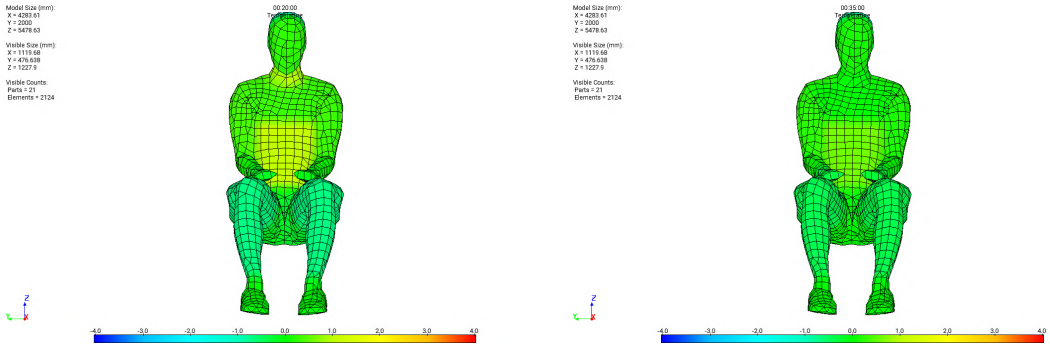

(a) Thermal sensation after 20 min. **(b)** Thermal sensation after 35 min.

Figure 4.27: Thermal sensation of the manikin in the winter clothing case.

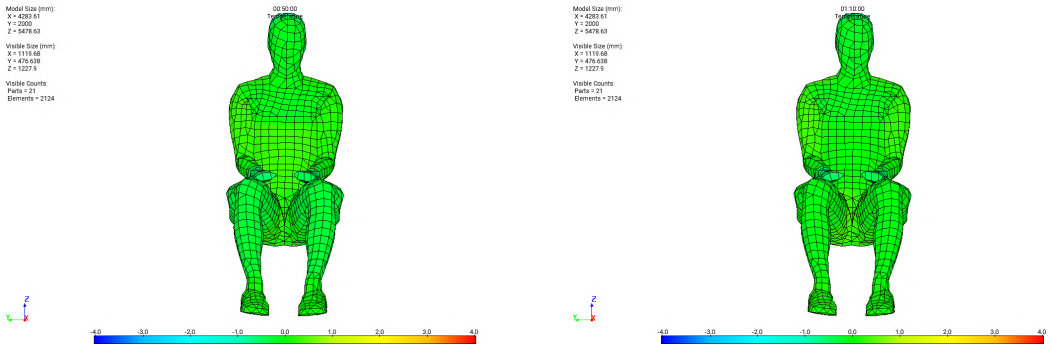

(a) Thermal sensation after 50 min. **(b)** Thermal sensation after 70 min.

Figure 4.28: Thermal sensation of the manikin in the winter clothing case.

In Figures 4.29 and 4.30 the skin temperature of the face, back, upper abdomen and lower legs is depicted. When analyzing the graphs, it can be seen that the skin temperatures of the upper abdomen and back are very similar. This is expected, since the same clothing is applied to both areas. Furthermore, it can be seen that the temperature is decreasing rapidly at the beginning, the same observation that was made for the heating case in Section 4.3. The results in Figure 4.29a also show the lowest temperature of the four body sections. This is also to be expected, since the face skin is exposed to the cabin air without any thermal insulation, unlike the other body parts.

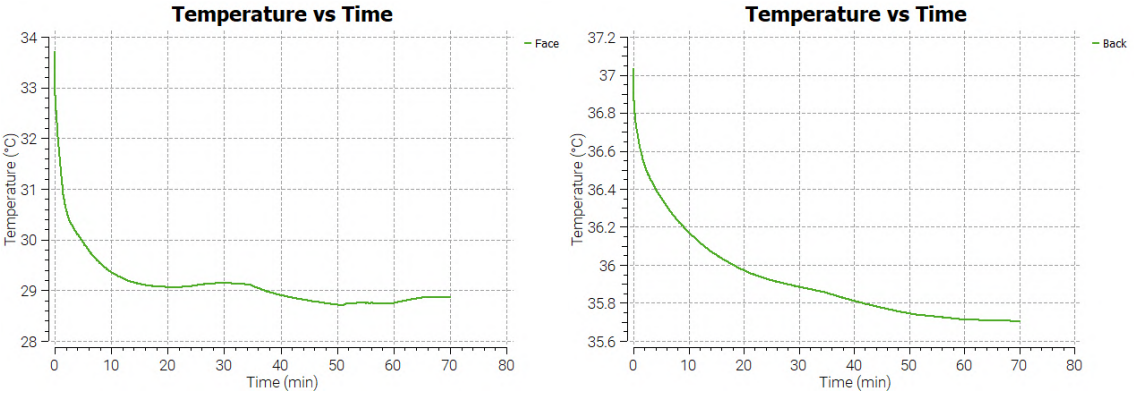

(a) Average skin temperature on the face. **(b)** Average skin temperature on the back.

Figure 4.29: Average skin temperature of the manikin.

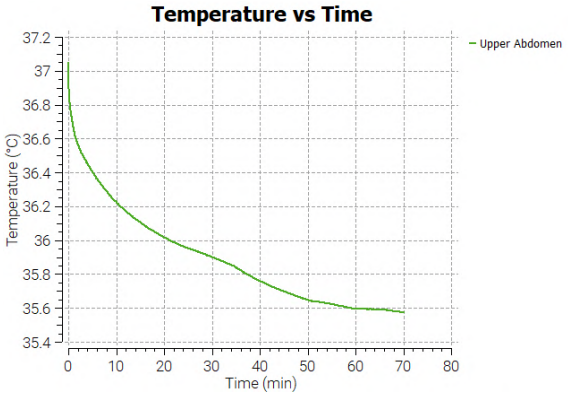

(a) Average skin temperature on the upper abdomen.

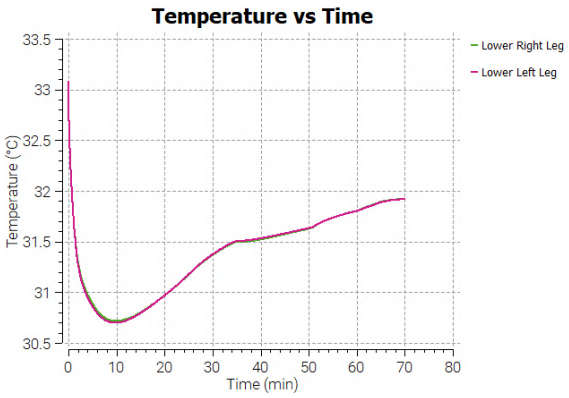

(b) Average skin temperature on the legs.

Figure 4.30: Average skin temperature of the manikin.

In Figures 4.31 to 4.34 the local thermal comfort on the face, back, upper abdomen, and lower legs are presented for the winter clothing case.

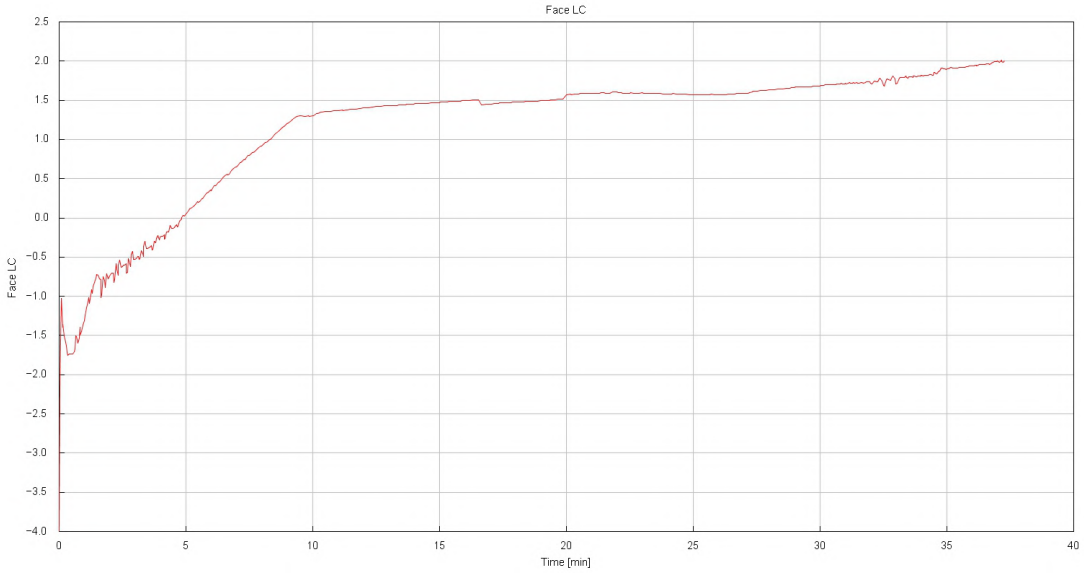

Figure 4.31: Thermal comfort on the face.

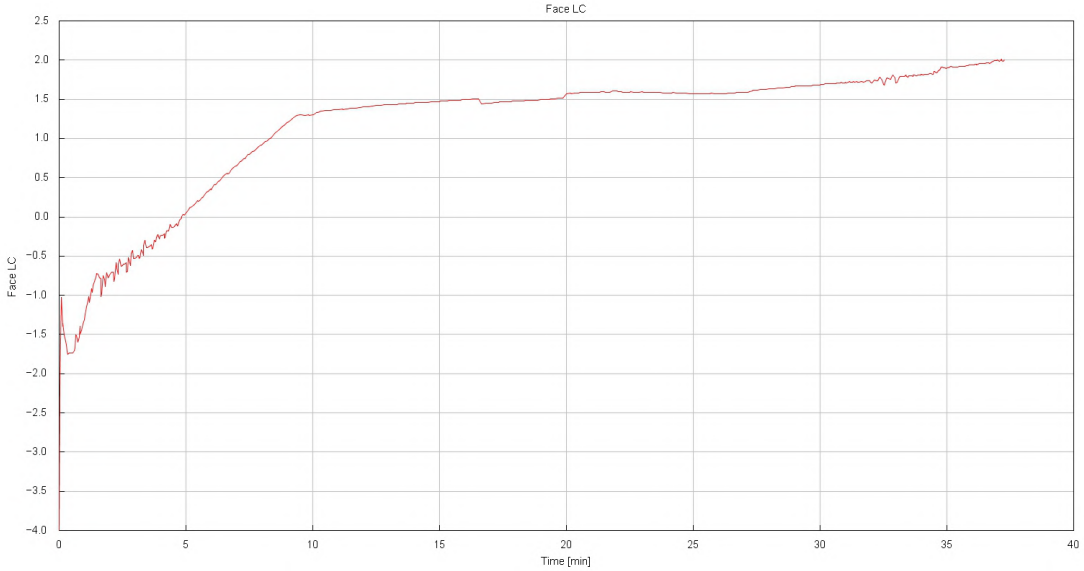

Figure 4.32: Thermal comfort on the back.

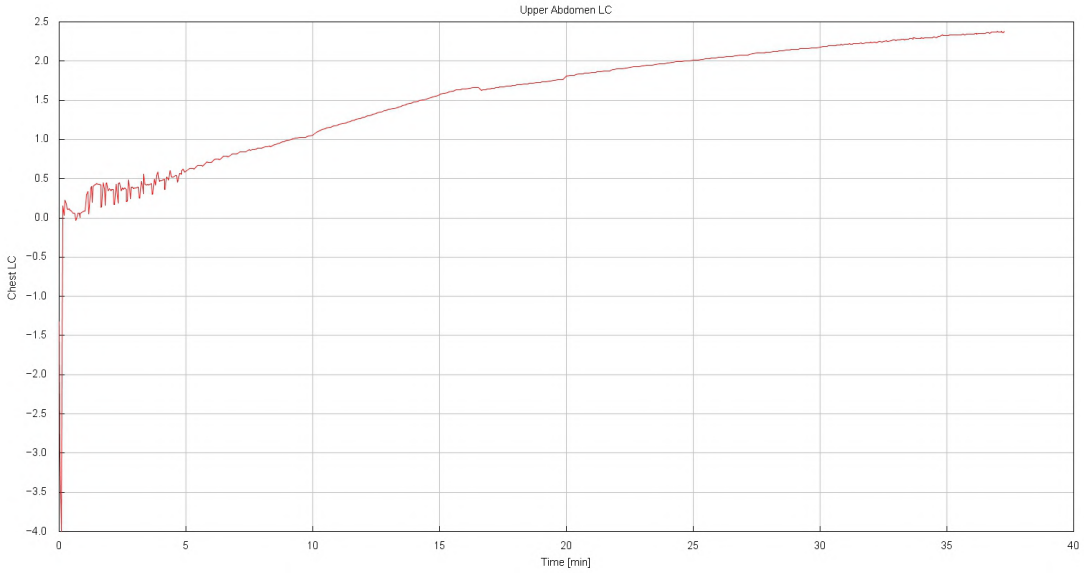

Figure 4.33: Thermal comfort on the upper abdomen.

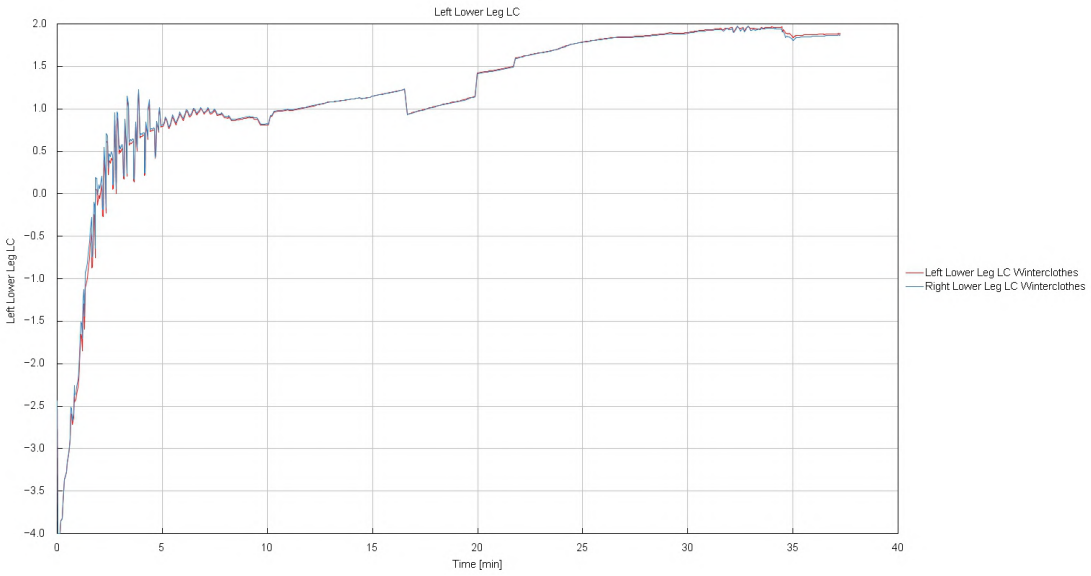

Figure 4.34: Thermal comfort on the lower legs.

Once again, it can be observed that the thermal comfort increases rapidly at the beginning of the simulation. Furthermore, it is seen that both the back and the upper abdomen never perceive negative comfort values, which is very positive. However, the face and lower legs perceive negative values at first, but reach positive thermal comfort values rather quickly. In the end of the simulation duration, the thermal comfort for the presented body segments is close to a value of 2, which is rather good.

The selected characteristics of different components of the simulation system are portrayed in Figures 4.35 and 4.36. In Figure 4.35a, the condenser energy rate is visualized. It can be observed that the energy rate is quite stable for the first 30 minutes. Thereafter, there is a change in the driving cycle and the level adjusts. As seen in Figure 4.35a there are some instabilities at the end of the simulation duration. This will be discussed in more detail in Section 4.6, but is likely caused by the climate control model and its interaction with the developed cabin model as they are two-way coupled. The same kind of behavior can be seen for the auxiliary load of the system in Figure 4.35b.

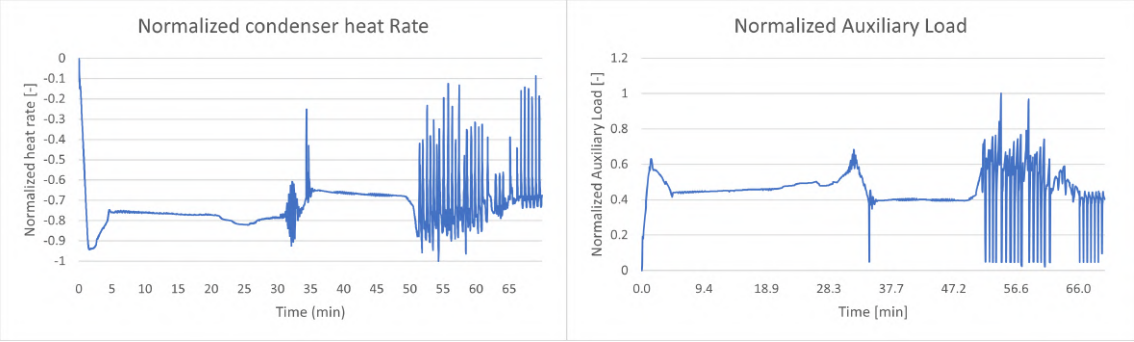

(a) Condenser energy rate. **(b)** Auxiliary load of the system.

Figure 4.35: Performance of the thermal system.

It can be seen in Figure 4.36a that the battery temperature decreases at the beginning of the simulation. Thereafter, it reached a stable level that was maintained for the remainder of the first 30 minutes of the driving cycle. Then it decreases further before increasing again. The results at the end of the duration are likely affected by the instabilities observed in the other graphs. As for the volume averaged cabin temperature seen in Figure 4.36b, the same characteristics can be seen as for the heating case. First, the temperature increases rapidly before reaching a stable temperature. After the driving cycle changes, the temperature decreases slightly before increasing again once the instabilities at the end of the duration are apparent.

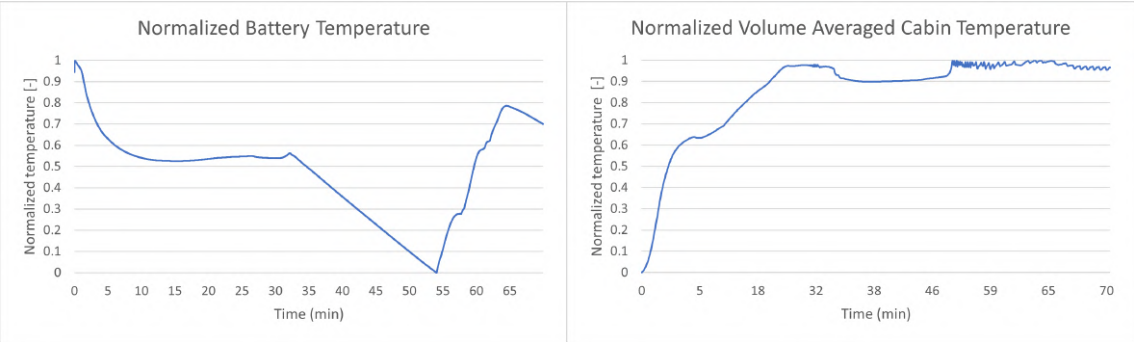

(a) Average battery temperature. **(b)** Volume averaged cabin temperature.

Figure 4.36: Temperature of the system components.

4.6 Comparison between the simulation cases

In Figures 4.37 and 4.38 a comparison between skin temperatures is visualized for the two simulation cases. An interesting observation made from the figures is that the skin temperature of the thermal manikin is higher when wearing winter clothing, although the cabin is climatized to a temperature that is 4°C lower than in the heating case. This is happening because the winter clothing has higher thermal insulation than the clothes used in the heating case. Furthermore, this confirms the theory behind the winter clothing case; it may be possible to heat the cabin to a lower temperature while still obtaining adequate thermal comfort for the passengers and thereby also saving energy.

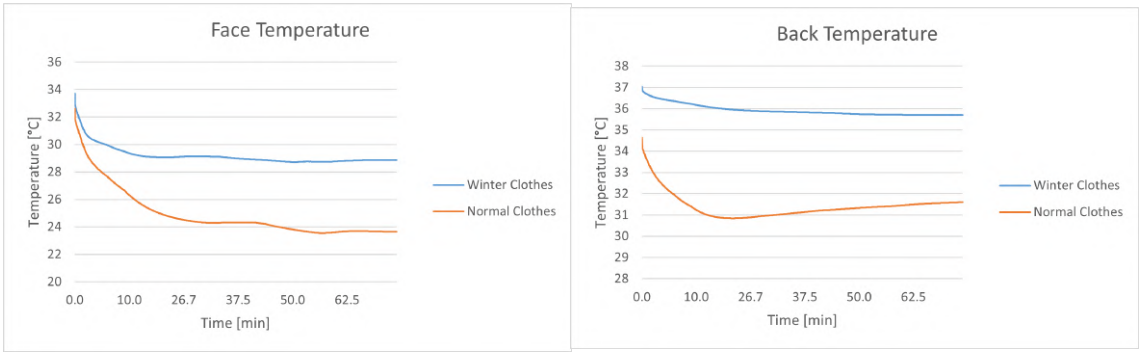

(a) Face temperatures. **(b)** Back temperatures.

Figure 4.37: Comparison between average skin temperatures.

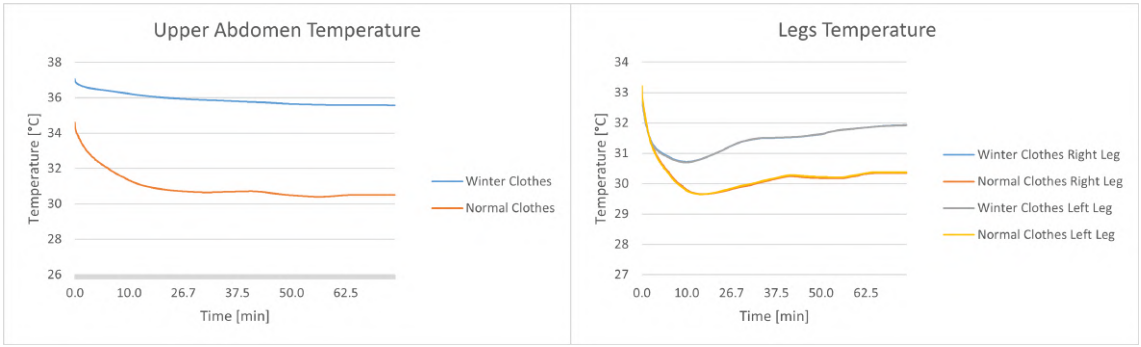

(a) Upper abdomen temperatures. **(b)** Lower leg temperatures.

Figure 4.38: Comparison of average skin temperatures.

Another confirmation of this can be observed in Figure 4.39, where the thermal comfort after 35 minutes is compared for the two cases. It is evident from the results that the overall thermal comfort is higher for the thermal manikin wearing winter clothing. The same observation can also be made for the other time steps, when comparing the results seen in Figures 4.4-4.6 with the results in Figures 4.23-4.25.

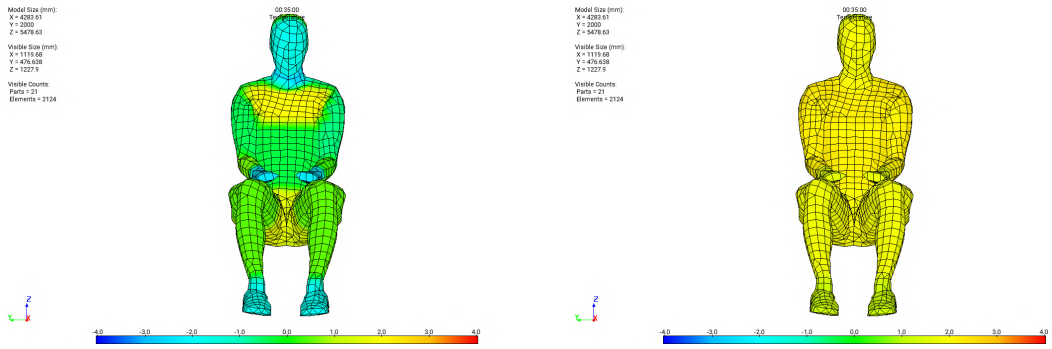

(a) Normal clothes. **(b)** Winter clothes.

Figure 4.39: Comparison of thermal comfort for the two cases.

The same can be seen in Figure 4.40 below, where the overall thermal comfort of the two simulation cases is compared to each other. Furthermore, comparison of the

local thermal comfort for the individual body segments is presented in Appendix A and a comparison of local thermal sensation between the two cases is found in Appendix B.

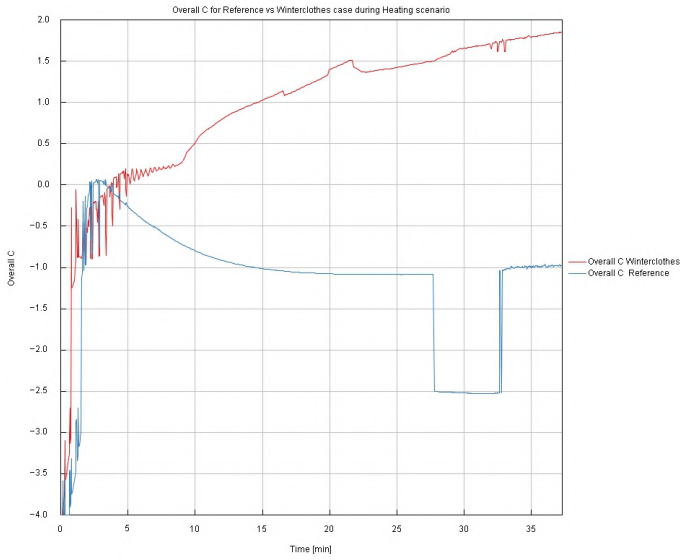

Figure 4.40: Comparison of the overall comfort perceived by the thermal manikin for the two simulation cases.

Unfortunately, it can be seen in Figure 4.40 that some unrealistic behavior is occurring for the heating case after approximately 27 minutes. It is difficult to explain exactly what is causing this, but since it is an average, some discrepancy in a local value could be the cause. In addition to that, it can be observed that the overall thermal comfort perceived by the thermal manikin is significantly higher for the case with winter clothing, similar to what has been seen in the previous figures.

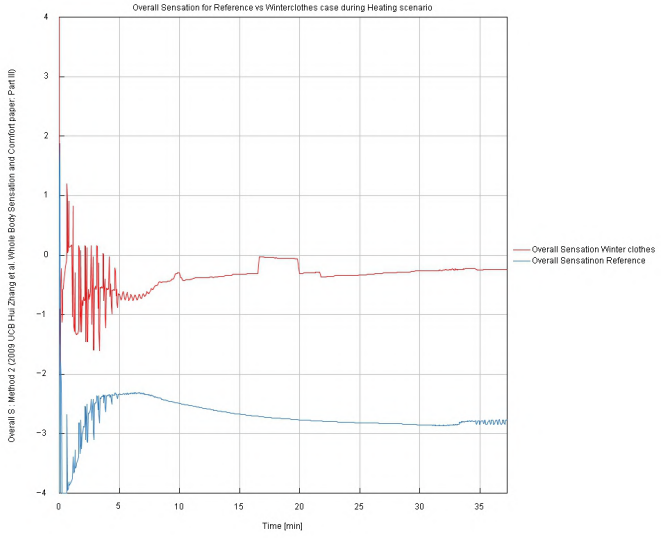

Figure 4.41: Comparison of the overall sensation perceived by the thermal manikin for the two simulation cases.

Similarly, in Figure 4.41, it is seen that the thermal sensation is significantly higher for the winter clothing case compared to the heating case. Furthermore, when analyzing the graphs portrayed in Appendix A and B, it is generally true that the thermal sensation is more stable than the thermal comfort. This may be explained by comparing Equations 2.13 and 2.14 where it is seen that the thermal comfort equation is much more complex than that of the thermal sensation.

Furthermore, the results of the lower climatization temperature can be observed in Figure 4.42a, where it can be seen that the simulation configuration used for the case with winter clothing has a lower auxiliary load than that of the heating case. This is expected, as the target average cabin temperature is 4 °C lower. A similar observation can be made in Figure 4.42b where it can be seen that the condenser energy rate is lower for the winter clothing case. This is the case since less heat transfer is needed in the condenser air, due to the lower cabin temperature target. However, it can also be seen that there are stability issues for the winter clothing simulation during the end of the driving cycle. This is likely due to the complexity of the complete system simulation environment, as well as its coupling to the climate control model. Instabilities were found to occur when targeting lower cabin temperatures when using the climate control model, but they have not been further investigated due to the project time constraints. Furthermore, this cabin modeling method is new and optimization of the settings may have to be made.

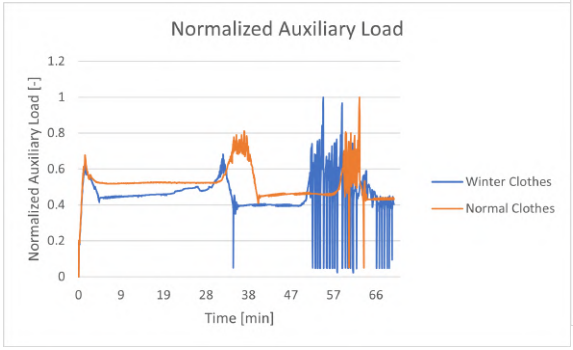

(a) Comparison of the auxiliary load.

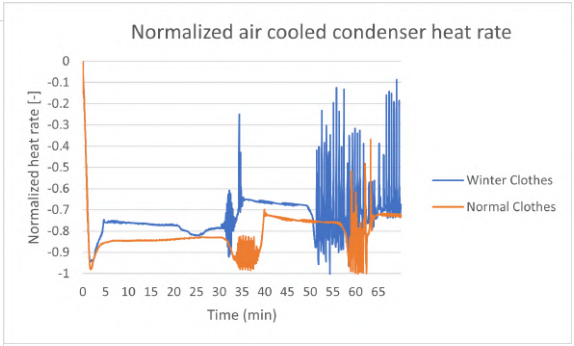

(b) Comparison of the condenser energy rate.

Figure 4.42: Graphs depicting comparisons between the two simulation cases.

Due to the stability issues observed at the end of the simulation, only the first 47 minutes of the simulation have been used for the rest of the analysis covered in the thesis. In Figure 4.43 the auxiliary load and the condenser heat rate can be seen, but for the shorter duration. The data obtained from the figure show that the auxiliary load is approximately 3.61% lower for the winter clothing case than for the heating case. Furthermore, the data in Figure 4.43b show that the condenser energy rate is about 9.57% lower for the winter clothing case than for the heating case. The thermal comfort results in combination with those of the auxiliary load confirm that there is a potential to save energy from cabin climatization if adjustment is made based on the type of clothing worn by the driver.

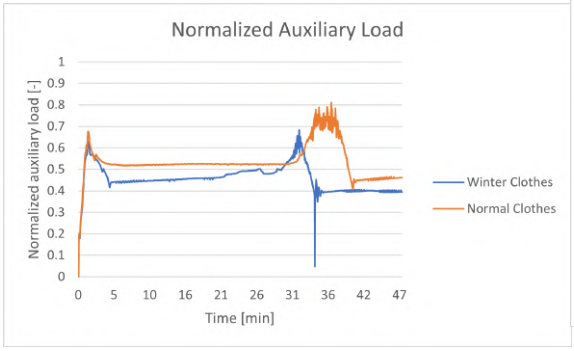

(a) Comparison of the auxiliary load.

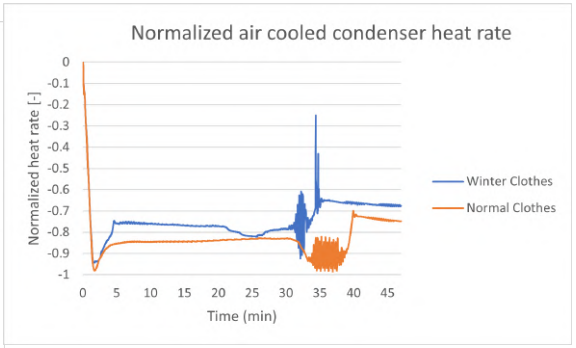

(b) Comparison of the condenser energy rate.

Figure 4.43: Graphs depicting comparisons between the two simulation cases for the shorter duration.

Lastly, a comparison of battery and cabin temperature for the two cases is presented in Figure 4.44. As seen in Figure 4.44a, the battery temperatures are very similar for the two cases. The major difference appears at the end of the duration where the temperature increases significantly for the winter clothing case. This may be caused by the instabilities in the climate control model, as the large temperature increase occurs at the same point of time as the instabilities. When instead looking at Figure 4.44b it can be observed that the two temperature curves are very similar. The main difference between the cases is that the cabin temperature is lower for the winter clothing case. This result is expected since the target temperature in the climate control model is set to a lower target for this case. Furthermore, another difference is the small oscillations that can be seen at the end of the winter clothing simulation, similar to the other results presented above.

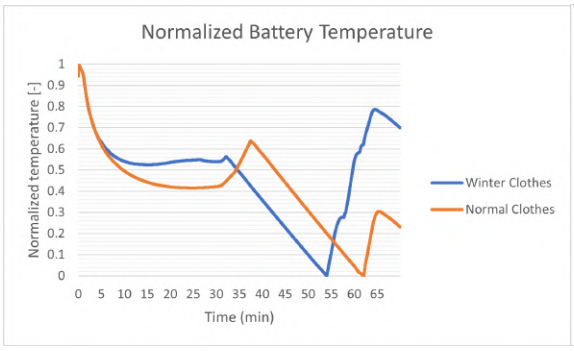

(a) Comparison of the average battery temperature.

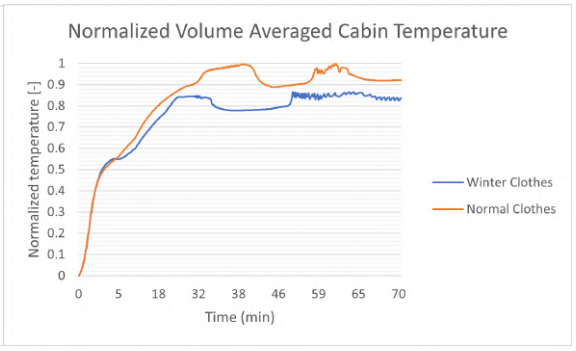

(b) Comparison of the volume averaged cabin temperature.

Figure 4.44: Graphs depicting comparisons between the two simulation cases.

5
Conclusion

The purpose of this thesis was to further develop the cabin simulation methodology used currently by CEVT. This was done by integrating a CFD solver for the cabin flow, which allows for a more detailed solution of the flow properties inside the cabin. This solution was then coupled with the thermal solver TAITherm to assess the thermal comfort of the passengers inside the vehicle cabin.

Altogether the results obtained from this thesis study are satisfactory and promise new levels of simulation accuracy for the cabin. However, there are areas of improvement that should be considered before considering this a mature methodology. A discussion of future work for this method can be found in Chapter 6. Furthermore, the implementation of thermal comfort analysis has shown that it can increase the energy efficiency of vehicles, and this method could have impacts on the way energy optimization of the climate is considered in the automotive industry.

To conclude this thesis, the method shows exciting new prospects when integrating the analysis of thermal comfort in thermal simulations of vehicle cabins, and I am excited to see how CEVT can use this method to develop the next generation of electromobility.

6
Future work

While the integration of this new methodology has been largely successful, there are several actions that can be considered for future work, using the findings from this thesis.

First, the possibility of optimizing the model with regard to time should be considered. The simulation models used in this thesis had a simulation time increase of about 11 times in comparison to the previously used method. Due to the time limitation of the thesis, this has not been addressed. However, it could be possible to achieve a reduction in computing time by adjusting the simulation setup settings. For example, adjusting the solver time steps could possibly speed up the simulation time.

A second consideration could be to adapt and develop the models to work for simulation cases concerning cooling scenarios as well. Furthermore, more advanced and realistic driving cycles should be tested as this may affect the stability of the models. Another prospect that needs to be considered is the validation data. At the time of the thesis, data from physical tests were not available to validate the simulation results. When data are available, the models must be validated and the accuracy of the model should be evaluated if this method is to be used in future development.

Moreover, further development of the methodology used in this thesis could be considered. For example, several new functions in newer releases of GT-SUTIE make the usage of the methodology much simpler. Signal- and parameter passing in GT-SUITE would simplify the modeling in GT-TAITherm tremendously, as changes could be made directly in GT-SUITE. Furthermore, the newer versions of GT-SUITE have improved the human modeling extension which allows for much simpler human modeling inside of GT-TAITherm.

Finally, it should be kept in mind that the stability of the simulations performed in this thesis was not optimal when targeting lower cabin temperatures. Therefore, the maturity of the method should be considered before using this methodology in future work at CEVT.

Bibliography

[1] Aakash30jan. Schematic illustration of the energy spectrum of turbulent energy cascade - https://commons.wikimedia.org/wiki/File:Schematic-illustration-of-the-energy-spectrum-of-turbulent-velocity-cascade.png; 2017.

[2] Hemmati S, Doshi N, Hanover D, Morgan C, Shahbakhti M. Integrated cabin heating and powertrain thermal energy management for a connected hybrid electric vehicle. Applied Energy. 2021;283.

[3] White FM. Fluid Mechanics seventh edition by Frank M. White. Power. 2011.

[4] Andersson B, Andersson R, Håkansson L, Mortensen M, Sudiyo R, Van Wachem B. Computational fluid dynamics for engineers. vol. 9781107018952; 2011.

[5] Versteeg HK, Malalasekera W. Computational Fluid Dynamics: The Finite Volume Method. vol. M; 2007.

[6] Incropera FP, DeWitt DP, Bergman TL, Lavine AS. Incropera's principles of heat and mass transfer. Wiley. 2017.

[7] Zhang H, Huizenga C, Arenas E, Wang D. Thermal sensation and comfort in transient non-uniform thermal environments. European Journal of Applied Physiology. 2004;92(6).

[8] Ashrae. Thermal Environmental Conditions for Human Occupancy. ANSI/ASHRAE Standard 55-2004. 2004;2004.

[9] Edel Z. EV Modeling Capabilities of TAITherm; 2021.

[10] Convergent Science. Converge 2.4 Manual; 2017.

[11] B Cain BF, Osczevski R. The concept and theoretical considerations of a cold weather clothing system. Ottawa: Protective Sciences Division; 1998.

[12] Wu YS, Fan JT, Yu W. Effect of posture positions on the evaporative resistance and thermal insulation of clothing. Ergonomics. 2011;54(3).

A

Comparison of thermal comfort

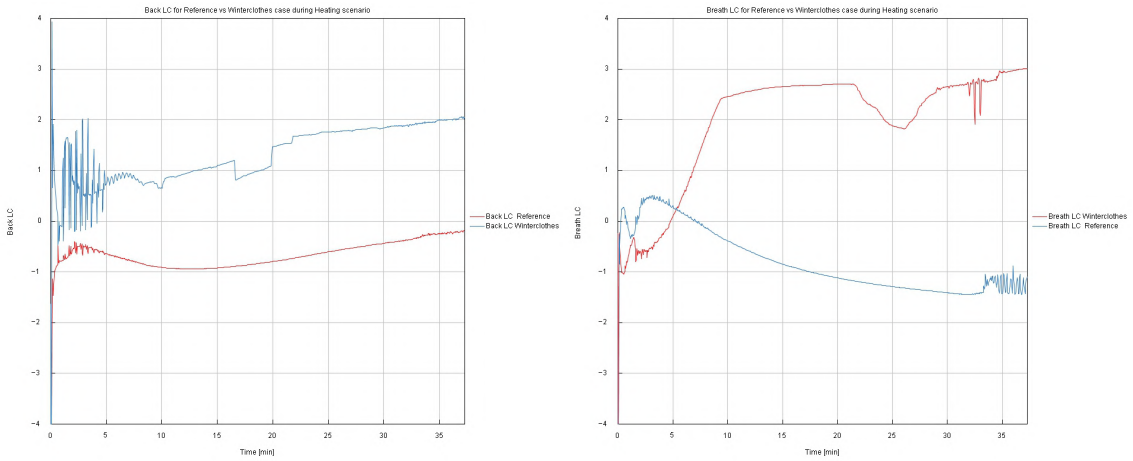

(a) Local thermal comfort on the back. **(b)** Local thermal comfort on breath level.

Figure A.1: Comparison of local thermal comfort for the two simulation cases.

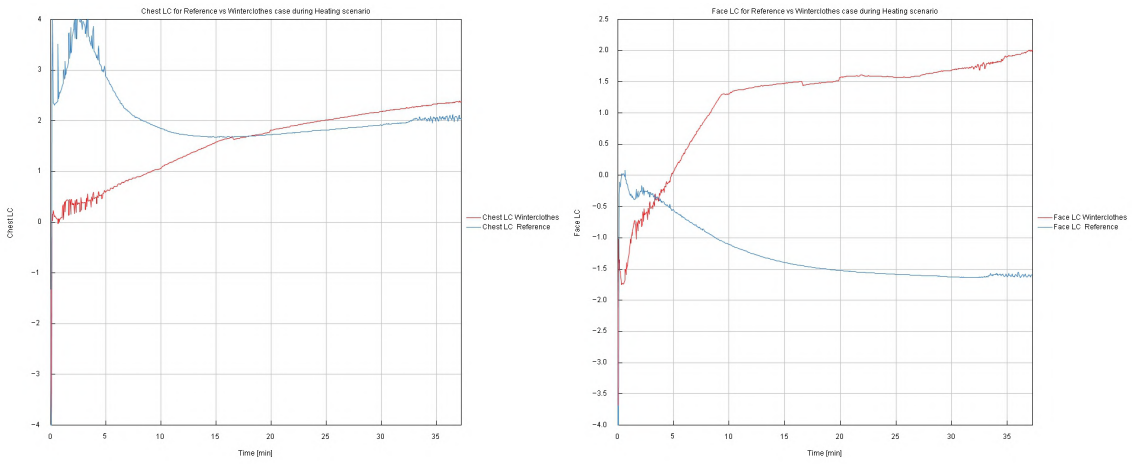

(a) Local thermal comfort on the chest. **(b)** Local thermal comfort on the face.

Figure A.2: Comparison of local thermal comfort for the two simulation cases.

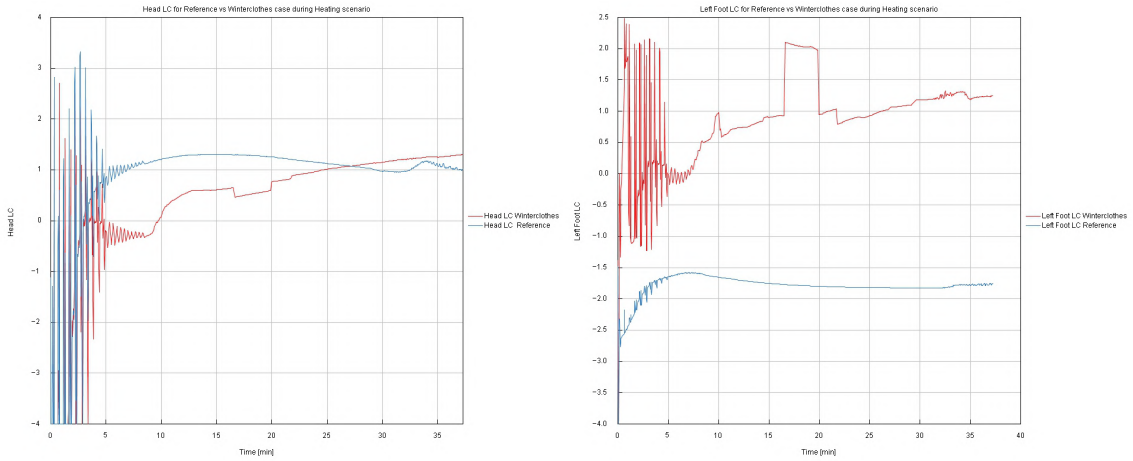

(a) Local thermal comfort on the head. **(b)** Local thermal comfort on the left foot.

Figure A.3: Comparison of local thermal comfort for the two simulation cases.

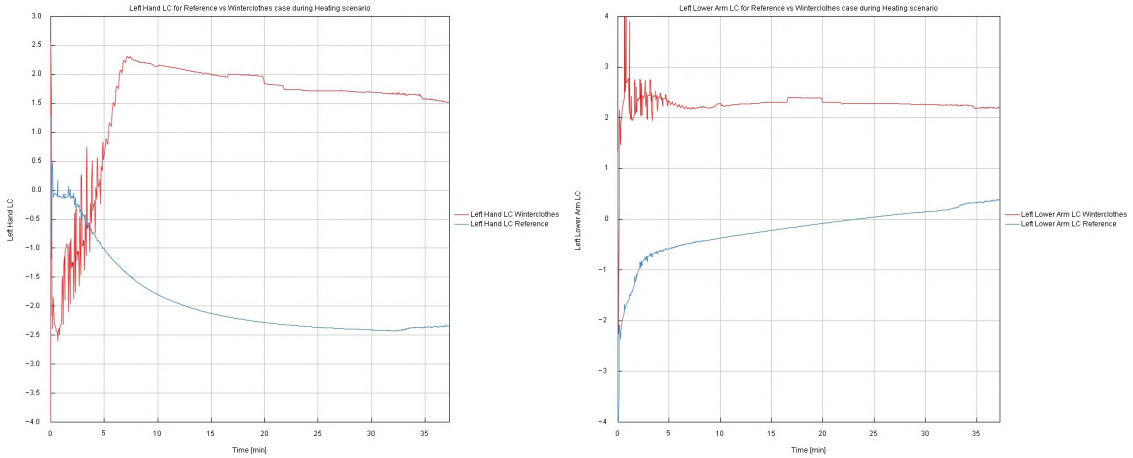

(a) Local thermal comfort on the left hand. **(b)** Local thermal comfort on the left lower arm.

Figure A.4: Comparison of local thermal comfort for the two simulation cases.

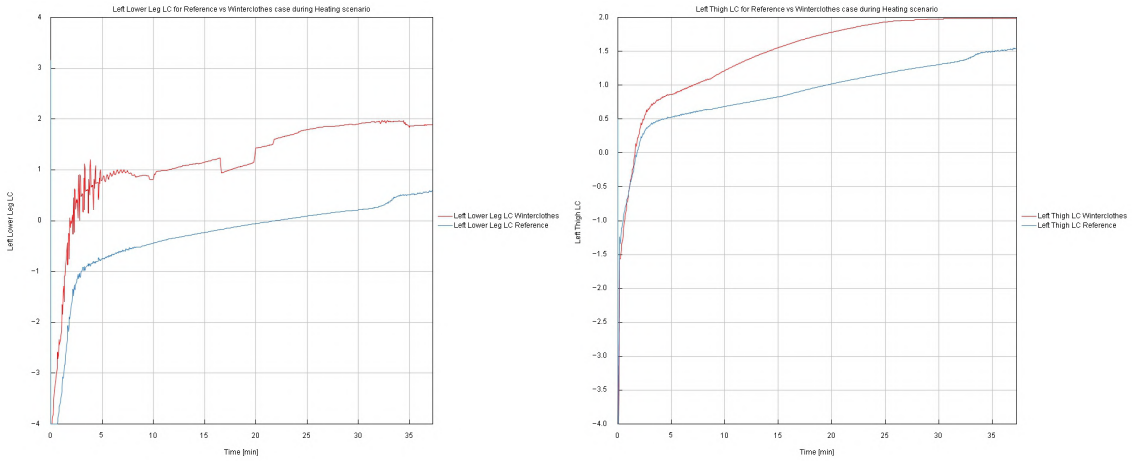

(a) Local thermal comfort on the left lower leg.

(b) Local thermal comfort on the left thigh.

Figure A.5: Comparison of local thermal comfort for the two simulation cases.

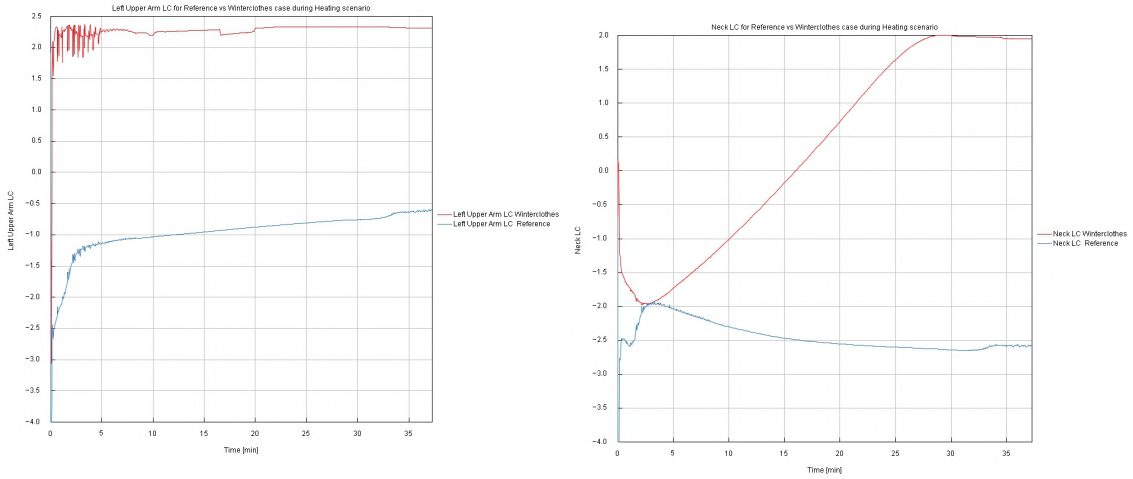

(a) Local thermal comfort on the left upper arm.

(b) Local thermal comfort on the neck.

Figure A.6: Comparison of local thermal comfort for the two simulation cases.

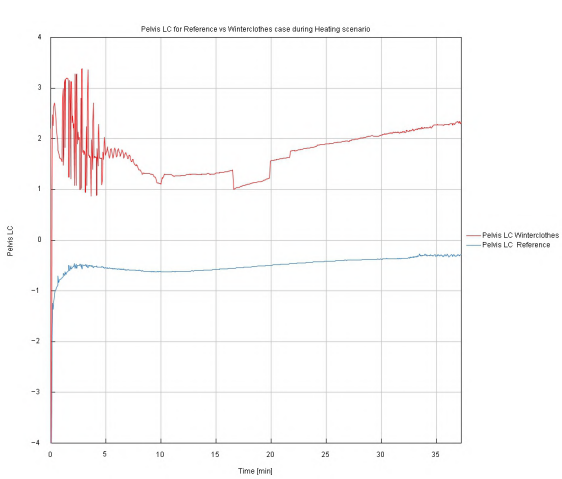

(a) Local thermal comfort on the pelvis.

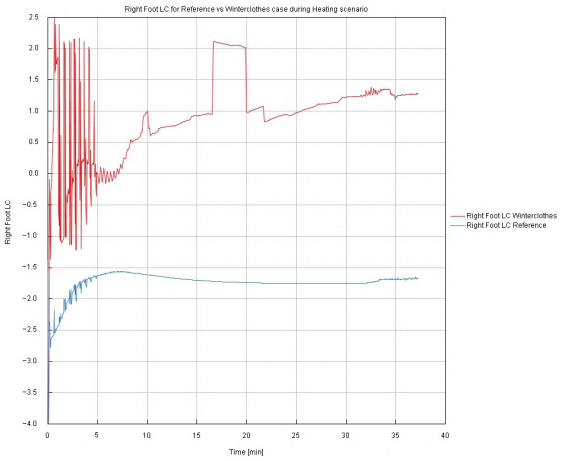

(b) Local thermal comfort on the right foot.

Figure A.7: Comparison of local thermal comfort for the two simulation cases.

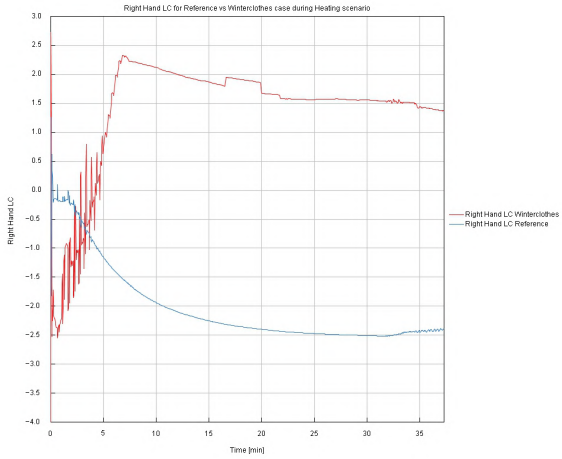

(a) Local thermal comfort on the right hand.

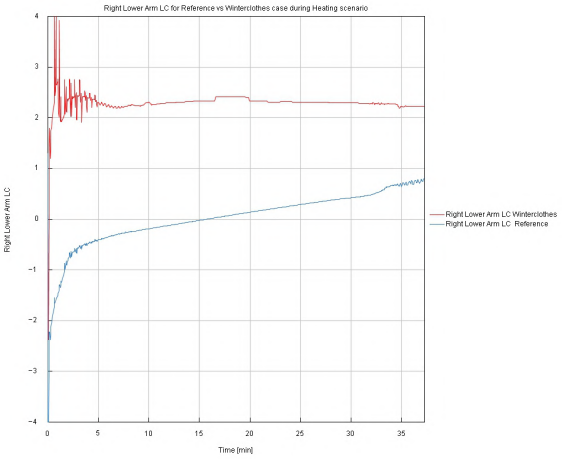

(b) Local thermal comfort on the right lower arm.

Figure A.8: Comparison of local thermal comfort for the two simulation cases.

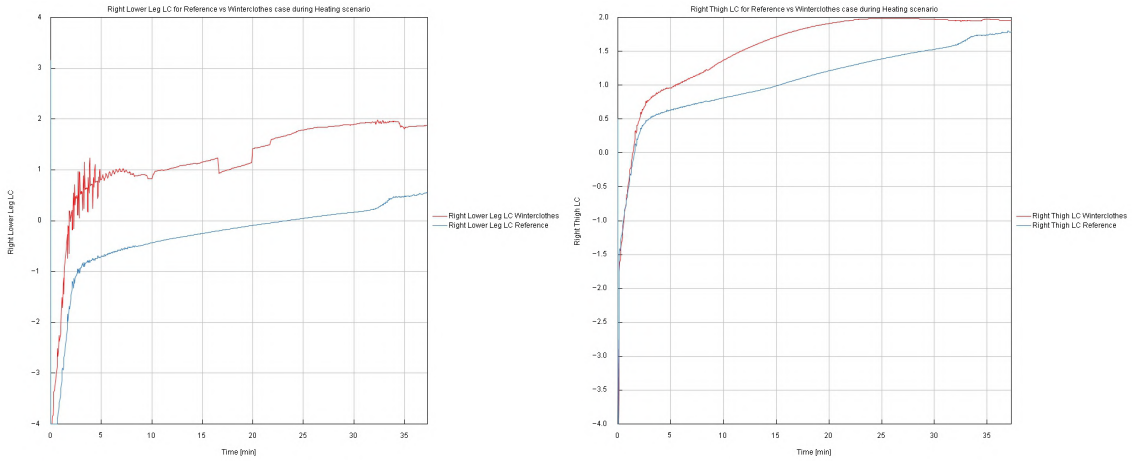

(a) Local thermal comfort on the right lower leg.

(b) Local thermal comfort on the right thigh.

Figure A.9: Comparison of local thermal comfort for the two simulation cases.

B

Comparison of thermal sensation

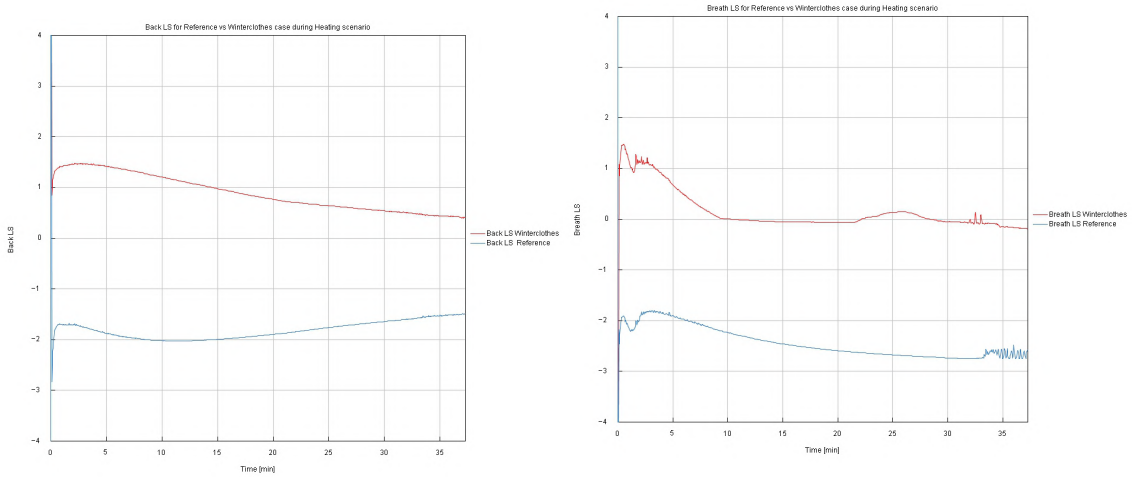

(a) Local thermal sensation on the back. **(b)** Local thermal sensation on breath level.

Figure B.1: Comparison of local thermal sensation for the two simulation cases.

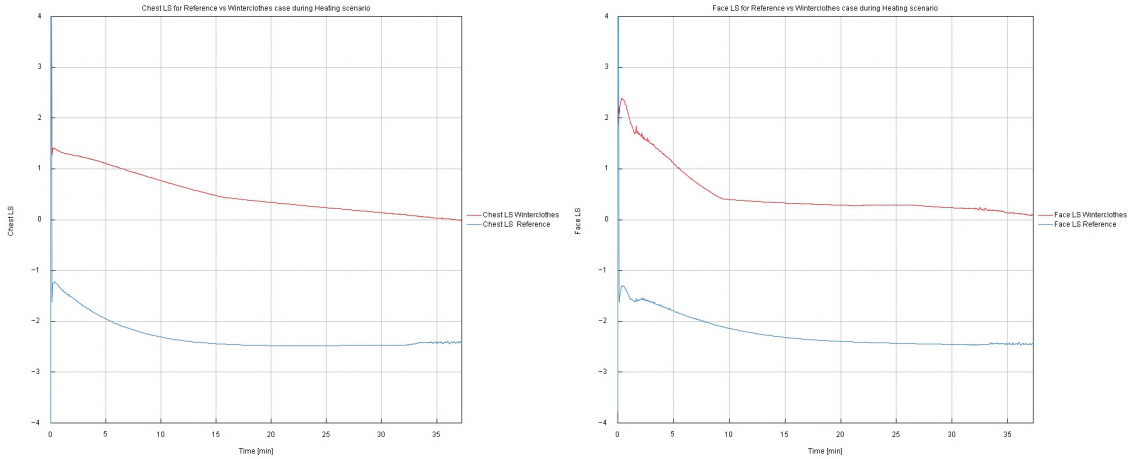

(a) Local thermal sensation on the chest. **(b)** Local thermal sensation on the face.

Figure B.2: Comparison of local thermal sensation for the two simulation cases.

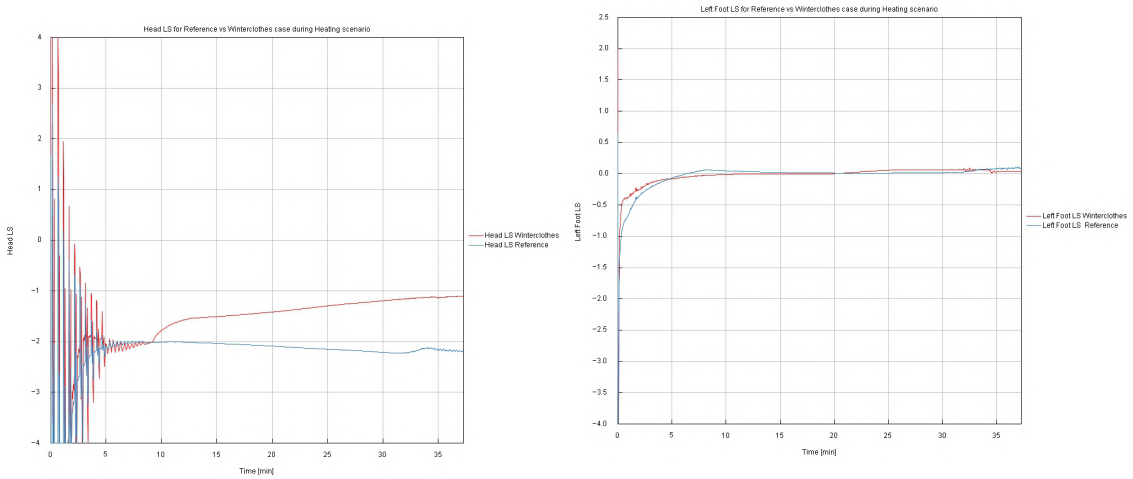

(a) Local thermal sensation on the head.

(b) Local thermal sensation on the left foot.

Figure B.3: Comparison of local thermal sensation for the two simulation cases.

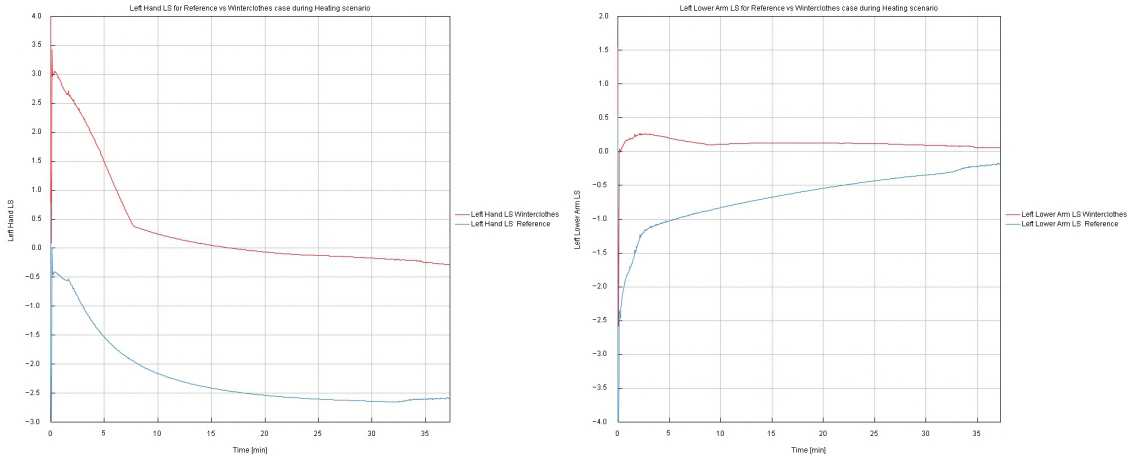

(a) Local thermal sensation on the left hand.

(b) Local thermal sensation on the left lower arm.

Figure B.4: Comparison of local thermal sensation for the two simulation cases.

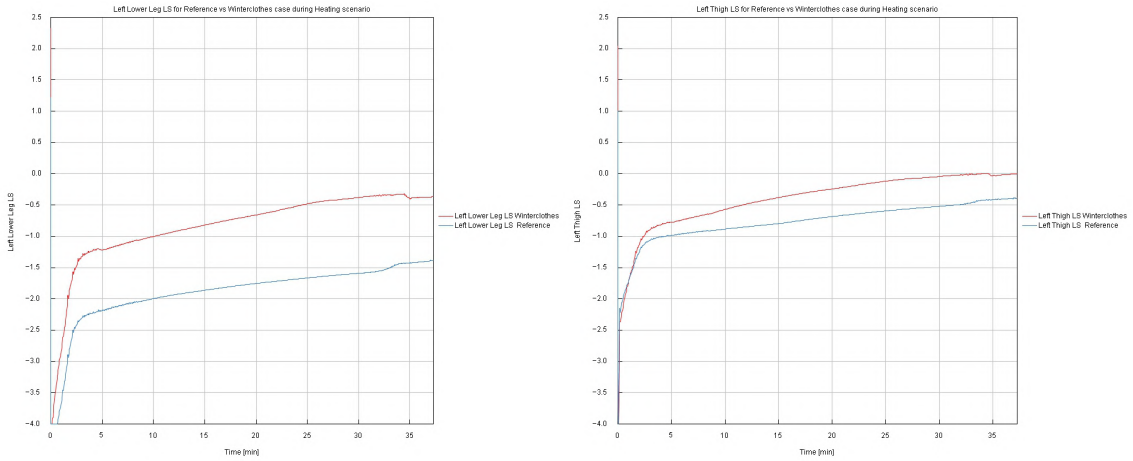

(a) Local thermal sensation on the left lower leg.

(b) Local thermal sensation on the left thigh.

Figure B.5: Comparison of local thermal sensation for the two simulation cases.

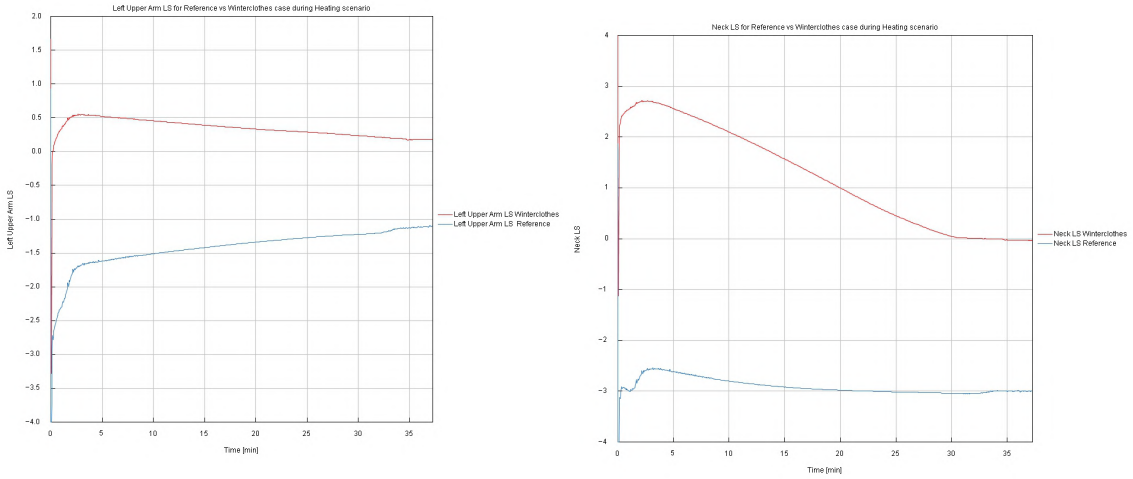

(a) Local thermal sensation on the left upper arm.

(b) Local thermal sensation on the neck.

Figure B.6: Comparison of local thermal sensation for the two simulation cases.

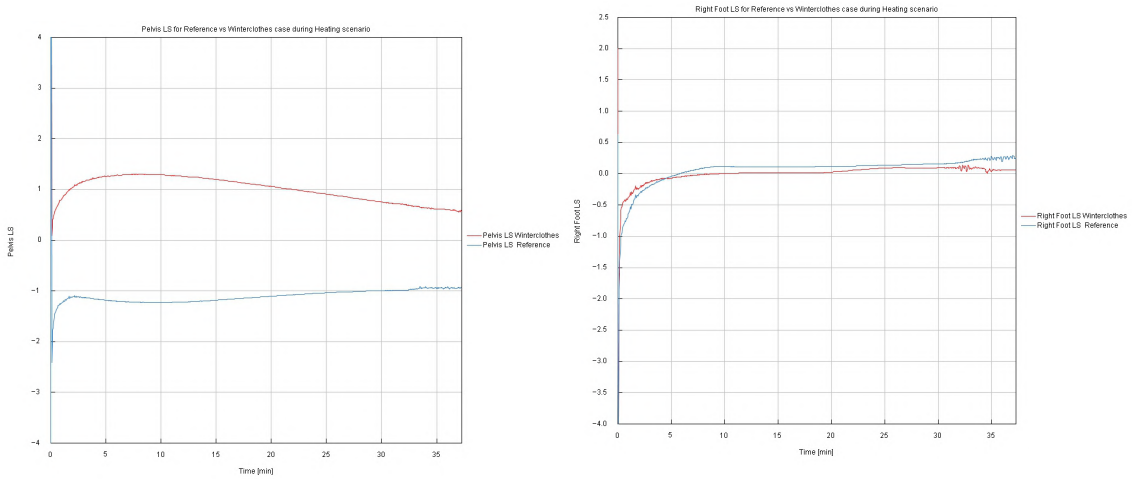

(a) Local thermal sensation on the pelvis.

(b) Local thermal sensation on the right foot.

Figure B.7: Comparison of local thermal sensation for the two simulation cases.

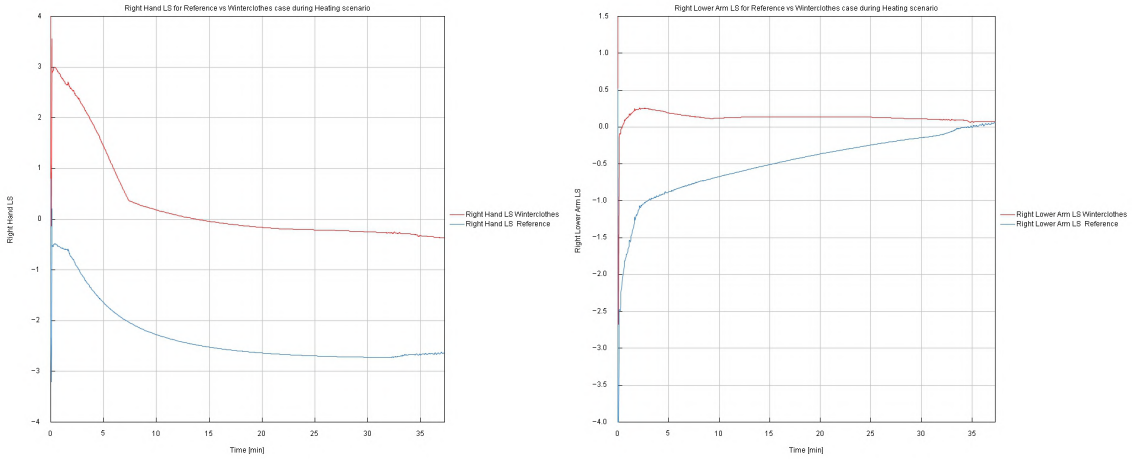

(a) Local thermal sensation on the right hand.

(b) Local thermal sensation on the right lower arm.

Figure B.8: Comparison of local thermal sensation for the two simulation cases.

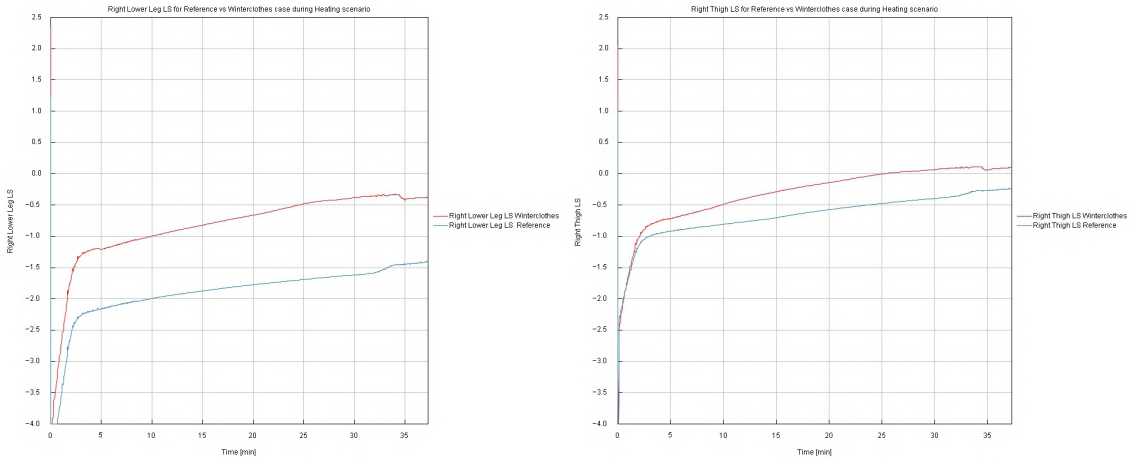

(a) Local thermal sensation on the right lower leg.

(b) Local thermal sensation on the right thigh.

Figure B.9: Comparison of local thermal sensation for the two simulation cases.

DEPARTMENT OF MECHANICS AND MARITIME SCIENCES
CHALMERS UNIVERSITY OF TECHNOLOGY
Gothenburg, Sweden
www.chalmers.se

CHALMERS
UNIVERSITY OF TECHNOLOGY